Stable carbon-isotope record of shallow-marine evaporative epicratonic basin carbonates, Ordovician Williston Basin, North America

ANTUN HUSINEC* and STIG M. BERGSTRÖM†

Department of Geology, St. Lawrence University, 23 Romoda Drive, Canton, NY 13617, USA (E-mail: ahusinec@stlawu.edu)
†*Division of Earth History, School of Earth Sciences, The Ohio State University, 125 S. Oval Mall, Columbus, OH 43210, USA*

Associate Editor – Adrian Immenhauser

ABSTRACT

Secular variations in stable carbon-isotope values of marine carbonates are used widely to correlate successions that lack high-resolution index fossils. Various environmental processes, however, commonly may affect and alter the primary marine carbon-isotope signal in shallow epicratonic basins. This study focuses on the marine carbon-isotope record from the carbonate–evaporite succession of the upper Katian (Upper Ordovician) Red River Formation of the shallow epicratonic Williston Basin, USA. It documents the carbon-isotope signal between the two major Ordovician positive shifts in $\delta^{13}C$, the early Katian Guttenberg and the Hirnantian excursions. Eight $\delta^{13}C$ stages are identified based on positive excursions, shifts from positive to negative values and relatively uniform $\delta^{13}C_{carb}$ values. A correlation between carbon-isotope trends and the relative sea-level changes based on gross facies stacking patterns shows no clear relation. Based on the available biostratigraphy and $\delta^{13}C$ trends, the studied Williston Basin curves are tied to the isotope curves from the North American Midcontinent, Québec (Anticosti Island) and Estonia, which confirm the Late Katian age (*Aphelognathus divergens* Conodont Zone) of the upper Red River Formation. The differences in the $\delta^{13}C$ overall trend and absolute values, coupled with the petrographic and cathodoluminescence evidence, suggest that the carbon-isotope record has been affected by the syndepositional environmental processes in the shallow and periodically isolated Williston Basin, and stabilized by later burial diagenesis under reducing conditions and the presence of isotopically more negative fluids.

Keywords $\delta^{13}C$ chemostratigraphy, carbonate diagenesis, Ordovician, sequence stratigraphy, Williston Basin.

INTRODUCTION

The Ordovician has traditionally been considered to have been dominated by greenhouse conditions (Fischer, 1982; Frakes *et al.*, 1992) with warm temperatures, high sea-level, and an atmospheric pCO$_2$ level estimated to be between eight and 22 times higher than today (Yapp & Poths, 1992; Berner, 1994; Berner & Kothavala, 2001; Herrmann *et al.*, 2004; Vandenbroucke *et al.*, 2010). Such a relatively ice-free world of the Early Ordovician underwent cooling in the late Middle and early Late Ordovician (Pope & Read, 1998; Trotter *et al.*, 2008), culminating in the Hirnantian glaciation episode (Frakes, 1979; Brenchley *et al.*, 1994, 2003; Qing & Veizer, 1994; Paris *et al.*, 1995; Marshall *et al.*, 1997; Finnegan *et al.*, 2011) and mass extinction
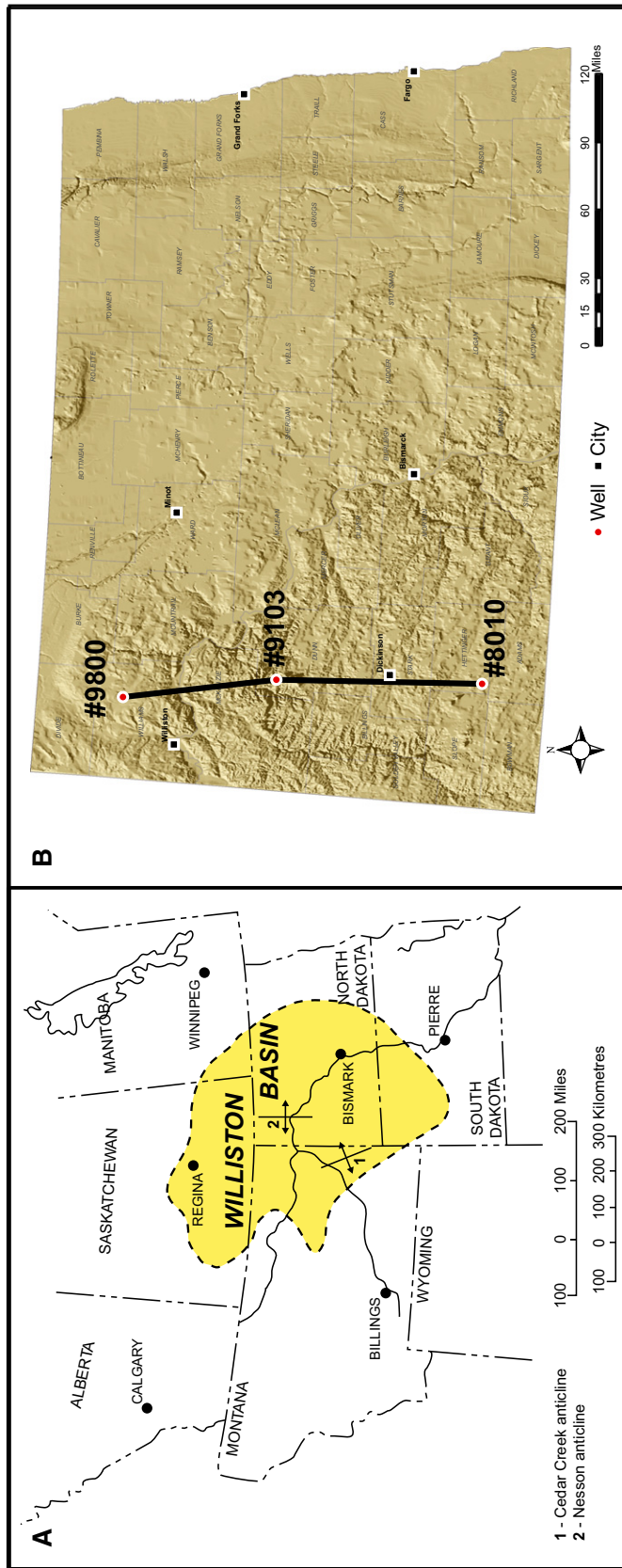
Fig. 1. Location map. (A) Map of central North America showing outline of Williston Basin (modified from Carlson & Anderson, 1965). (B) Map of North Dakota showing locations of the three wells used in this study.

events (Sepkoski, 1995; Sheehan, 2001; Alroy *et al.*, 2008; Bergström *et al.*, 2014). The Hirnantian glaciation was preceded by enhanced organic carbon burial during the Chatfieldian that resulted in the Guttenberg excursion, which was associated with lowered atmospheric pCO_2 to levels near the threshold for ice buildup (Saltzman & Young, 2005). Both of these episodes are marked by significant positive shifts in carbon-isotope values (Saltzman & Young, 2005, and references therein). Interestingly, although examined in detail in Baltoscandia (e.g. Kaljo *et al.*, 2008; Ainsaar *et al.*, 2010; Bergström *et al.*, 2010b), relatively little is known in North America about the $\delta^{13}C$ trend in the interval between these prominent excursions. The only available $\delta^{13}C$ curves from North America that partially cover this interval are the Midcontinent composite curve (Bergström *et al.*, 2007, 2010d), the Anticosti Island curve (Young *et al.*, 2010) and the Monitor Range composite curve from central Nevada that was constructed by Saltzman & Young (2005) based partly on data from Kump *et al.* (1999). To study the carbon-isotope signal of this interval in more detail, three continuously cored wells through the Upper Ordovician Williston Basin shallow-marine carbonate–evaporite Red River Formation were used.

The objectives of this study were to: (i) establish a detailed carbon-isotope stratigraphy for the Upper Ordovician study interval of the Williston Basin and thus provide a reference curve for the Late Katian interval between Guttenberg and the Hirnantian excursions; (ii) assess the influence of various environmental processes affecting and potentially altering the primary marine $\delta^{13}C$ signal in a shallow, evaporative epicratonic basin; as well as (iii) evaluate later diagenetic processes related to burial diagenesis, potentially resetting the $\delta^{13}C$ signal; and (iv) test whether the relation between carbon-isotope trends and sequence stratigraphy in the basin can be established.

GEOLOGICAL SETTING

The Williston Basin of North Dakota, South Dakota, Montana, Wyoming and south-central Canada is a kidney-shaped, Phanerozoic epicratonic depression in the western distal Canadian Shield (Fig. 1). An approximately 4900 m (16 000 ft) thick succession of sedimentary rocks spans the Cambrian through to Quaternary (e.g.

Carlson & Anderson, 1965; Gerhard *et al.*, 1982) and includes all the classic Sloss' (1963) unconformity bounded sequences in North America. The Palaeozoic sequences are mostly carbonates, which were deposited in dominantly shallow marine environments (Porter & Fuller, 1959; Carlson & Anderson, 1965; Gerhard *et al.*, 1982), occupying equatorial latitudes (Jin *et al.*, 2013) in a region of high evaporation as inferred from thick evaporite deposits. Of the several major epeirogenic structures within the basin, the Cedar Creek (Clement, 1987) and Nesson anticlines (Gerhard *et al.*, 1987; LeFever *et al.*, 1987) are the best known. Basin subsidence began in the Chatfieldian (early Katian) with the deposition of the Winnipeg Group (Oberg, 1966; Sweet, 1982) when the initial depression with seaway connections to the west was formed (Sandberg, 1964). During its Phanerozoic evolution, the basin has subsided *ca* 4900 m (16 000 ft) without undergoing severe orogenic deformation or significant peripheral tectonic distortion (Gerhard *et al.*, 1982).

Lithostratigraphy

The Upper Ordovician Red River Formation is present throughout the Williston Basin, reaching a maximum thickness of slightly more than 210 m (700 ft) in the central part of the basin in Dunn County, North Dakota (Fig. 2). The Red River Formation sharply overlies a series of argillaceous layers of predominantly siliciclastic deposits of the underlying early Katian (Chatfieldian) Winnipeg Group. The upper boundary of the Red River Formation with overlying carbonates and shales of the Stony Mountain Formation is also conformable, but sharp (Carroll, 1979; Fig. 2).

The Red River Formation consists primarily of shallow water limestone and dolomite, the latter having major oil reservoirs, and traditionally it has been subdivided into a lower and an upper unit (Sinclair, 1959; Fuller, 1961; Ballard, 1963; Carroll, 1979). The lower unit ranges from 120 to 170 m (400 to 550 ft) in thickness and is dominated by fossiliferous, bioturbated and selectively dolomitized wackestone (Porter & Fuller, 1959; Carroll, 1979). The upper 40 to 90 m (120 to 270 ft) thick unit is characterized by the presence of extensive evaporite capping cycles consisting of the basal fossiliferous limestone and fine-grained dolomite (Porter & Fuller, 1959; Carroll, 1979). In addition, thin argillaceous beds overlying nodular anhydrite are traceable basinwide on
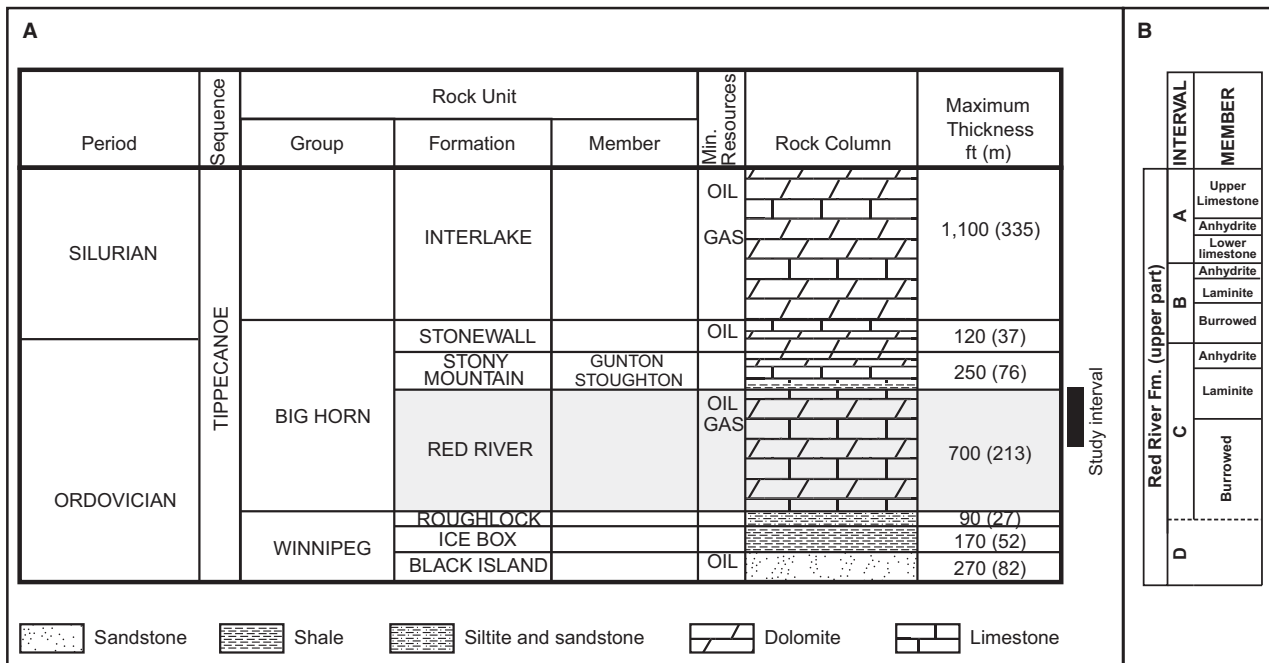
Fig. 2. (A) Stratigraphic column of the Tippecanoe sequence in North Dakota. Stratigraphic position of Upper Ordovician Red River Formation is highlighted (modified from Bluemle *et al.*, 1981; Murphy *et al.*, 2009). (B) Stratigraphic position of informal units within the studied upper Red River Formation (modified from Kohm & Louden, 1978; Carroll, 1979).

gamma-ray wireline logs. In the oil industry terminology, there are four porosity zones within the upper unit, in descending order, the 'A', 'B', 'C' and 'D' cycles (Kohm & Louden, 1978; Carroll, 1979). The first three of these comprise subtidal (burrowed) and intertidal (laminated) facies overlain by evaporites (anhydrites; Fig. 2B). The 'D' cycle occurs in porous dolomitized lenses in the lower, burrowed unit, below the 'C' cycle (e.g. Carroll, 1979; Longman *et al.*, 1983; Derby & Kilpatrick, 1985). Each cycle can be correlated basinwide using wireline logs.

There are no outcrops of the Red River Formation in the central Williston Basin but locally fossiliferous exposures are known along the basin margins in Wyoming (e.g. Holland & Patzkowsky, 2009) and southern Manitoba (e.g. Jin & Zhan, 2001). The lithostratigraphy of the Upper Ordovician in the outcrop areas, as well as in the subsurface of Alberta and Satskatchewan, is illustrated in Fig. 3. For a more detailed version of the stratigraphy, see Jin & Zhan (2001).

Biostratigraphy

There is some agreement that the combination of chemostratigraphy and biostratigraphy, where feasible, results in a more robust interpretation of the carbon-isotope curve. This approach is particularly important in such cases as the present one in which carbon-isotope data are available from a vertical succession of rather limited stratigraphic range.

The present study, with focus on a carbon-isotope stratigraphy of the Red River Formation, is based on samples from 70 to 87 m thick drillcore intervals just below the basal portion of the Stony Mountain Formation. The investigated interval, which represents *ca* 40% of the total thickness of the Red River Formation, is likely to be coeval with the Fort Garry, and possibly part of the Selkirk, members of the Red River Formation of Manitoba (Jin, 2000; Jin & Zhan, 2001; Fig. 3). The age of this succession has not been controversial and this interval has generally been referred to the Richmondian (upper Katian) Stage.

Regarding correlations with other well-studied locations in western North America, the B burrowed member of the Red River Formation has been correlated with part of the Horseshoe Mountain Member of the Bighorn Dolomite (Jin & Zhan, 2001; Boyd, 2007; Rendall & Husinec, 2012), the lower Coronach Member of the Herald Formation of Saskatchewan and the middle Fort Garry Member of Manitoba (cf. Elias *et al.*, 1988). The latter authors also assigned the C
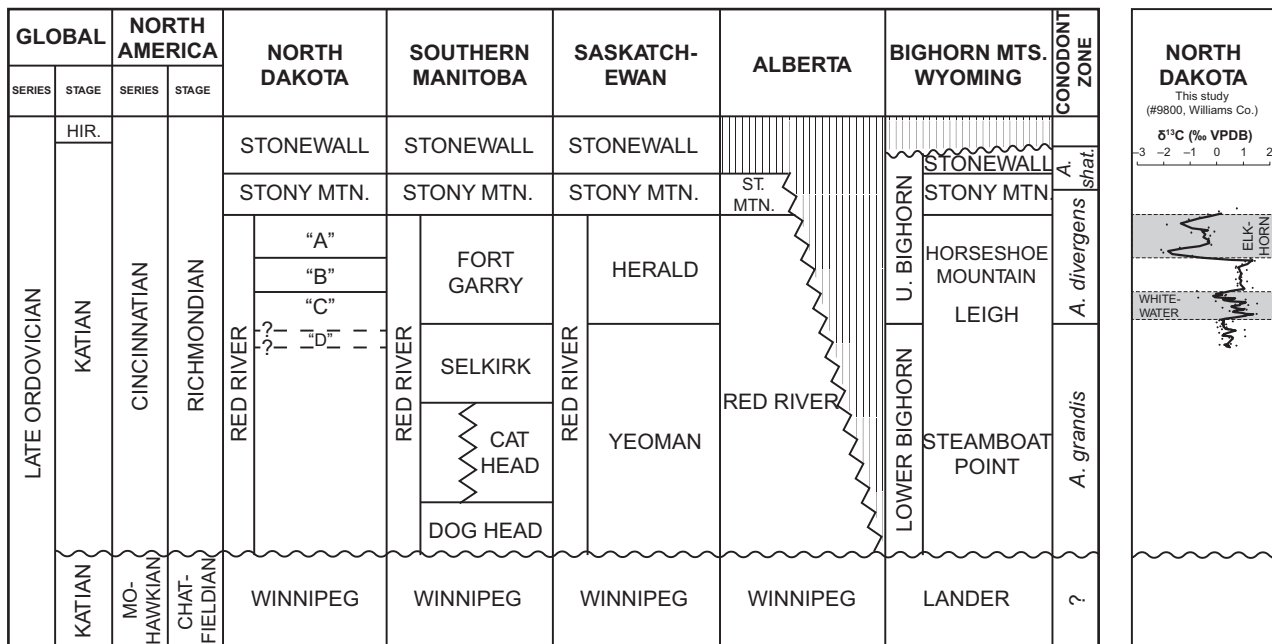
Fig. 3. Diagram illustrating global and North American series, formations and members recognized in the Williston Basin and adjacent areas. Note the prominent unconformity between the top of the Chatfieldian Winnipeg Group and the base of overlying Richmondian strata that corresponds to at least the entire Edenian and Maysvillian stages. Red River $\delta^{13}C$ curve (three-point moving average, core #9800, Williams County) with Cincinnati positive $\delta^{13}C$ excursions (Bergström *et al.*, 2007, 2010c) is on the right side of the figure. Abbreviation: Hir., Hirnantian.

laminite, the C anhydrite and the B burrowed members to the middle–upper Richmondian *Aphelognathus divergens* Conodont Zone that corresponds to the middle part of the *Amorphognathus ordovicicus* Conodont Zone.

In summary, because the sampled interval herein is in the upper half of the Red River Formation, it is likely to be coeval with an interval well above the base of the type Richmondian, probably above the Waynesville Formation in the Richmondian type area in the Cincinnati region. This conclusion is important for the interpretation of excursions in the $\delta^{13}C$ curves.

STUDY METHODS

This study is based on a detailed bed by bed analysis of three cores through the subsurface upper Red River Formation along the north–south transect in western North Dakota (Fig. 1). This transect includes the Simpson #1 core located roughly in the centre of the Willison Basin, as well as the Federal #10-1 and Urlacher State Unit #1 cores, the sites of which are located 104 km and 243 km, respectively, to the south from that of Simpson #1 (Appendix Table A1).

The cores were logged using a binocular microscope and stratigraphic position, pore types, mineralogy, sedimentary structures, textures, Dunham rock types, dolomite crystal sizes and fossils were recorded. Samples were taken at irregular intervals for petrographic and cathodoluminescence analyses as part of a larger study on high-resolution sequence stratigraphy and diagenesis of the Red River Formation. The above cores were selected because they were the thickest and stratigraphically most complete cores of the Red River Formation available at the Wilson M. Laird North Dakota Geological Survey's Core Laboratory in Grand Forks, which is the major core storage facility in the study region. No cores were available from the lower Red River Formation because that part of the formation is not a petroleum reservoir and, consequently, has not been the target of the drilling companies.

Two hundred and twenty-three samples of shallow-water carbonates from the upper Red River Formation were collected at intervals of between 30 cm and 90 cm from the three cores discussed above (Appendix Table A2). Fresh chips free of calcite veins, large fossil fragments and stylolites were drilled to obtain 0.5 g powdered bulk rock using a 1.8 mm regular car-

bide bur on a Dremel 400XPR rotary tool (Robert Bosch Tool Corporation, Mount Prospect, IL, USA). Bulk carbonate powders were analysed for stable isotopes ($\delta^{13}C$ and $\delta^{18}O$) using a common acid bath interfaced to a Finnigan-MAT 251 mass spectrometer (Finnigan-MAT, Bremen, Germany) at RSMAS/MGG Stable Isotope Laboratory of Peter Swart, University of Miami. The results are reported in permil relative to the VPDB (Vienna PeeDee Belemnite) standard. Reproducibility on replicate analyses was better than 0.1‰ for both carbon and oxygen isotopes.

Twelve non-covered thin sections representative of major facies from the studied cores were examined at the St. Lawrence Carbonate Sedimentology Laboratory using cathodoluminescence (CL) microscopy with a Technosyn coldcathodoluminescence unit (Reliotron control console; Reliotron Industries, Bedford, MA, USA) attached to an Olympus SZX-10 stereomicroscope (Olympus Corporation, Tokyo, Japan) equipped with an Olympus DP72 12.8MP digital colour camera. Operating conditions were 7 to 8 kV beam voltage and 0.6 to 0.8 mA beam current and chamber pressure 80 to 90 mTorr.

RESULTS

Depositional sequence framework

The facies in the upper Red River Formation in North Dakota are described and interpreted in Table 1. A generalized outline of the upper Red River sequence stratigraphy based on the three studied cores (Figs 4 to 6) is presented here to facilitate the discussion of: (i) the intrabasinal and extrabasinal correlation; and (ii) the relation between the carbon-isotope trends, relative sea-level and sequence stratigraphy. The sequence stratigraphic terminology in this paper follows the definitions of Van Wagoner *et al.* (1988) and Weber *et al.* (1995) for naming sequence stratigraphic depositional units and their component parasequences.

Long-term (third-order) depositional sequences

The upper part of the Red River Formation in Williston Basin, North Dakota, is made up of three complete longer term transgressive–regressive sequences (RR1, RR2 and RR3; Husinec, 2013) composed of lowstand (LST), transgressive (TST) and highstand systems tracts (HST); the top of the formation, i.e. the section stratigraphically above the A anhydrite (or A laminite where anhydrite is not present), probably represents a TST of the overlying sequence SM1 comprising shales of the Stony Mountain Formation. The absence of radiometric age data, and the difficulties in establishing precise intercontinental correlation based on established conodont, graptolite and brachiopod zones make estimation of the chronological duration of the sequences RR1 to RR3 difficult. Each of the upper Red River sequences RR1 to RR3 is characterized by unique, regionally correlative lithological properties, and by using neutron porosity and bulk density logs, these sequences can be traced regionally over North Dakota. Subaqueous anhydrites within each sequence probably formed during relative sea-level lows that lead to the precipitation of anhydrite in a quiet, lagoonal environment (e.g. Tucker, 1991; Sarg, 2001; and references therein). That the Red River anhydrites, which are restricted to central portion of the Williston Basin, are not lowstand wedges is suggested by their stratigraphic position in sequences RR1 to RR3, where they conformably overlie, are interbedded with and laterally pinch out against tidal flat laminites. In contrast, the restricted evaporite lowstand wedges overlie highstand systems tracts comprised of foreslope and basinal carbonate rocks (for example, the Paradox Basin: Hite & Buckner, 1981; Weber *et al.*, 1995). Within sequences, transgressive systems tracts are commonly thin and composed of subtidal, lagoonal facies of predominantly skeletal mudstone to wacke-packstone with abundant burrow mottling. The basal TST is at many locations characterized by a thin microbial laminite that probably formed during the onset of regional transgression associated with dissolution of anhydrite. This, in turn, raised the incoming ocean-water salinities and locally facilitated cyanobacterial blooms and preservation of stratiform stromatolitic structures (cf. Husinec & Read, 2011). Highstand system tracts are generally thicker than TSTs and composed of peritidal, porous laminated dolomite. Sequence boundaries are characterized by onlap of shallow subaqueous evaporites (cf. Sarg, 1988), with locally developed subaerial and submarine erosional truncation marked by intraclast breccia interbedded with dololaminites below sequence boundaries. Consequently, all sequence boundaries, except the lower sequence boundary of RR1, were picked at the base of shallow subaqueous to supratidal anhydrite. The tops of evaporite packages represent transgressive surfaces that are easily traceable basinwide in cores, and

Table 1. Upper Katian Red River Facies, Williston Basin, North Dakota, USA.

Lithology (depositional environment)	Anhydrite (shallow hypersaline subaqueous to supratidal)	Intraformational breccia/conglomerate (shallow subtidal to intertidal)	Microbial laminite, planar laminite, dololaminite (tidal flat)	Thrombolite (shallow subtidal to low intertidal)	Ooid dolograinstone-packstone (shallow subtidal/intertidal shoal)	Skeletal grainstone-packstone (high-energy bank, sheet, and shoal)	Skeletal wackestone-packstone (moderately shallow subtidal along the down dip margin of tidal flats or low-energy tidal channel)	Burrowed muddy carbonates: lime mudstone to skeletal wackestone-floatstone, dolomudstone/wackestone (low-energy subtidal)
Thickness and stratigraphic occurrence	0.1–5 m thick units commonly interbedded with dololaminite; onlaps or pinches out against tidal flat units	Units 2–3 to 30 cm thick occur at bases of some shallowing-upward cycles; associated with pyritized hardgrounds at MFS, or laminites in late HST	0.05–7.50 m thick units occur in HSTs of sequences RR1–RR3 or interbedded with anhydrite in LSTs	Units 0.1–1.20 m thick	30–40 cm thick units occur only in late HST of sequence RR1 and latest LST of RR2	Units 0.1–1.20 m thick occur throughout sections; absent in sequence SM1	0.15–2.0 m units commonly cap burrowed muddy carbonates in sequences RR0 and RR1	Units 0.15–7.50 m thick occur throughout sections; predominate in TST of sequences RR1–RR3
Colour	White to dark grey	Dark grey	Alternation of light grey and dark grey laminae	Light to dark grey	Dark grey	Brown to dark grey	Brown or brown with grey mottles if burrowed	Colour mottling; lighter, brown (matrix), and darker, grey mottles (burrows)
Sedimentary structures	Massive to nodular with chicken-wire fabric, flat lamination, less common convolute laminae	Sharp base and gradational top in subtidal setting; lamination in intertidal	Wavy and flat lamination, desiccation cracks; anhydrite nodules and crystal laths, rare silicified nodules	Cryptalgal clotted structure lacking lamination	Structureless	Structureless	Structureless or burrowed; rare cross-lamination	Extensive bioturbation (burrow mottling; abundant pyrite staining on hardgrounds, common stylolites and wispy kerogenous seams, nodular fabric, anhydrite crystals, rare mudcracks
Depositional texture and grain types	Anhydrite nodules from 5 mm to several centimetres in diameter	Several millimetre to centimetre-long angular clasts in grainstone matrix. Intraclasts reworked from tidal flats or shallow offshore areas	Poorly sorted, mud to granule-sized. Skeletal grains, rare intraclasts	Millimetre to centimetre-scale micrite clots surrounded by skeletal mudstone to wacke-packstone	Well-sorted, medium to coarse sand-size ooids	Range from well-sorted to poorly sorted, fine sand to granule-sized. Skeletal fragments, scarce intraclasts	Poorly sorted, mud matrix with sand-sized to rare granule-sized grains. Skeletal fragments, scarce intraclasts	Poorly sorted muds with fine sand to granule-sized grains. Skeletal fragments, rare micrite intraclasts
Biota	None	None	Calcified cyanobacteria (*Girvanella?*), rare ostracods and brachiopods	Calcified cyanobacteria, crinoids, brachiopods, corals	None	Common crinoids, brachiopods, gastropods, corals, less common ostracods and bryozoans	Common crinoids and brachiopods, less common gastropods, bryozoans and green algae	Common brachiopods, crinoids, trilobites, less common corals, ostracods and green algae, scarce bryozoans

MFS, maximum flooding surface; HST, highstand systems tract; LST, lowstand systems tract; TST, transgressive systems tract.
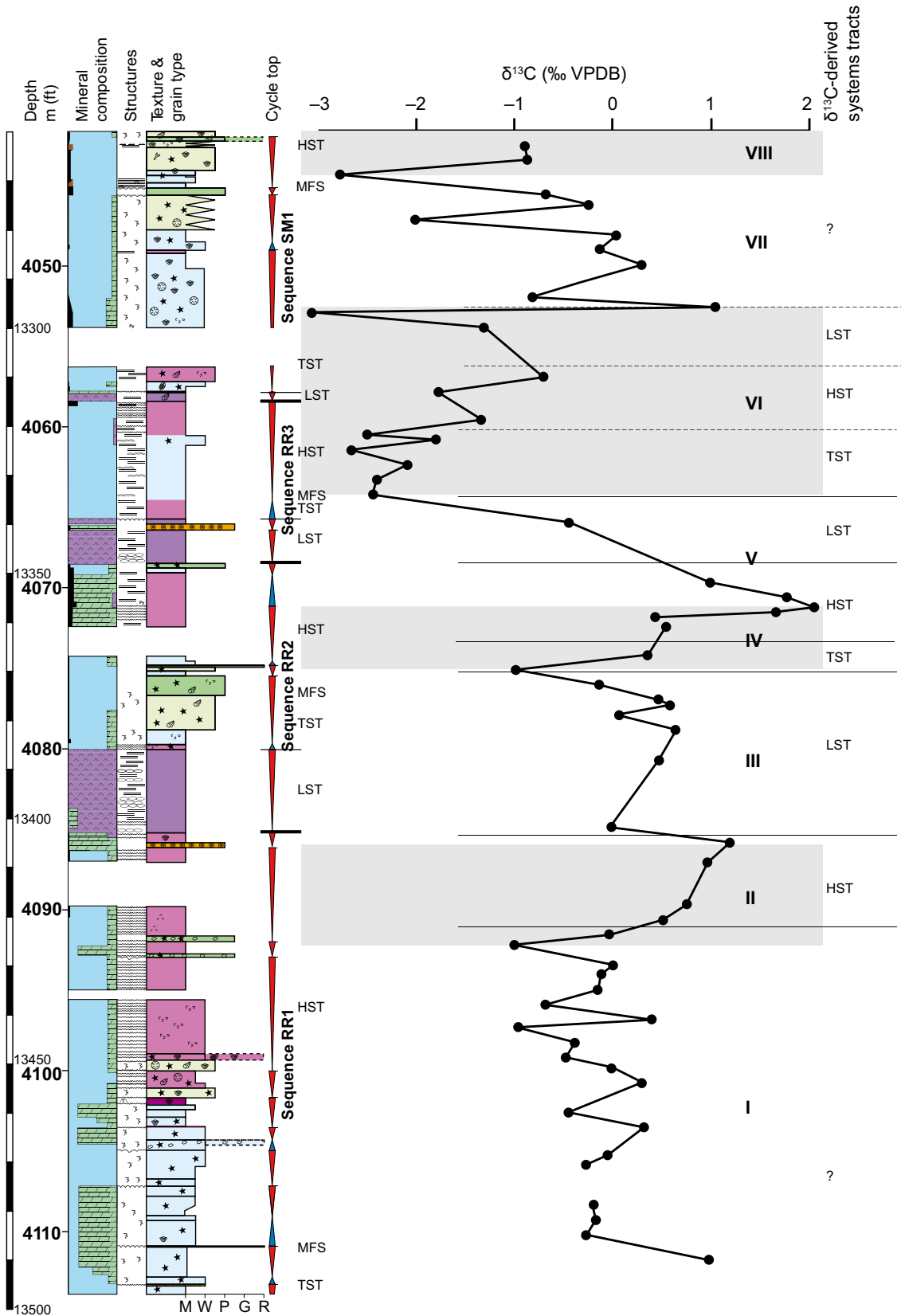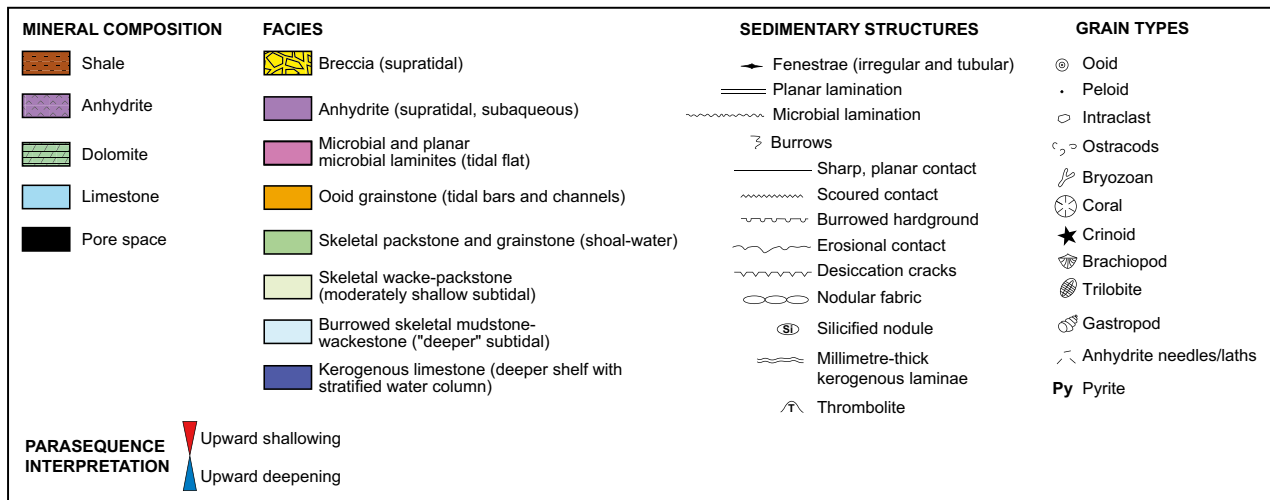
Fig. 4.

Fig. 4. Detailed stratigraphic column of core #9800 (Simpson #1, Williams County, North Dakota) showing mineral composition, sedimentary structures, Dunham rock types, parasequences and long-term depositional sequences. Upward-deepening units are shown by upward-narrowing triangles; upward-shallowing units are shown by upward-widening triangles. TST = transgressive systems tract, MFS = maximum flooding surface, HST = highstand systems tract, LST = lowstand systems tract. Carbon-isotope curve, carbon-isotope stages (Roman numerals) and δ^{13}C-derived systems tracts are on the right side of the figure. For well location, see Fig. 1.

especially on gamma ray logs, where they are characterized by a slightly positive excursion. These excursions are probably due to the presence of a very thin shale bed overlying the anhydrite. The shale was not recovered from any of the studied cores, so it can only be speculated if it represents an aeolian silt at the top of all observed LST deposits; alternatively, it can be interpreted to have been formed during initial invasion of marine waters into the shallow hypersaline Williston Basin during regional relative rises in sea-level (Weber *et al.*, 1995). Actual maximum flooding surfaces were difficult to locate in any of the cores and could only arbitrarily be picked based on broad characteristics, for example, above upward-decreasing and below upward-increasing shallow-water facies, beneath skeletal grainstones-packstones capping burrow-mottled muddy carbonates, or above repeated pyrite-encrusted hardgrounds.

Dolomite petrography and cathodoluminescence

Given the abundance and distribution of dolomite within the Red River Formation (Figs 4 to 6), to use the bulk carbonate matrix at 30 to 90 cm intervals for carbon and oxygen stable isotope analysis, both muddy limestone and laminated dolomite were sampled. To better understand the Red River dolomite diagene-

sis, its petrography is summarized below, and augmented with petrographic and cathodoluminescence (CL) observations reported herein.

Unlike the laminated members that are dolomitized pervasively, the burrowed members of the Red River Formation exhibit a complex and regionally discontinuous pattern of dolomitization (Kendall, 1976; Longman *et al.*, 1983; Holmden, 2009). Most commonly, as is the case in the study area, the burrows are dolomitized and the matrix is not; however, in other parts of the Williston Basin, both the burrows and the matrix can be dolomitized, or they both remain as limestone (Kendall, 1976; Longman *et al.*, 1983; Neese, 1985; Canter, 1998; Qing *et al.*, 2001; Gingras *et al.*, 2004). Dolomite is predominantly replacive and in laminated members occurs as non-planar, bimodal (5 to 50 μm) crystals in completely dolomitized intervals, or as 25 to 50 μm rhombs floating in lime mudstone or associated with stylolites (Zenger, 1996). In burrowed members, dolomite is composed of 20 to 160 μm, primarily non-planar crystals in the largely replaced burrow fills. It also occurs as crystals disseminated along stylolites, or less commonly as large crystals replacing echinoderm fragments, or as late-stage, void-filling saddle dolomite (Zenger, 1996). In the studied area, the two types of dolomite make up the bulk of the dolomite succession: aphanocrystalline to finely crystalline tidal-flat dolomite and finely to medium crystalline burrow-fill dolomite.

Fig. 5. Detailed stratigraphic column of core #9103 (Federal #10-1, Dunn County, North Dakota) showing mineral composition, sedimentary structures, Dunham rock types, parasequences and long-term depositional sequences. Upward-deepening units are shown by upward-narrowing triangles; upward-shallowing units are shown by upward-widening triangles. TST = transgressive systems tract, MFS = maximum flooding surface, HST = highstand systems tract, LST = lowstand systems tract. Carbon-isotope curve and carbon-isotope stages (Roman numerals) are on the right side of the figure. For key to symbols, see Fig. 4. For well location, see Fig. 1.
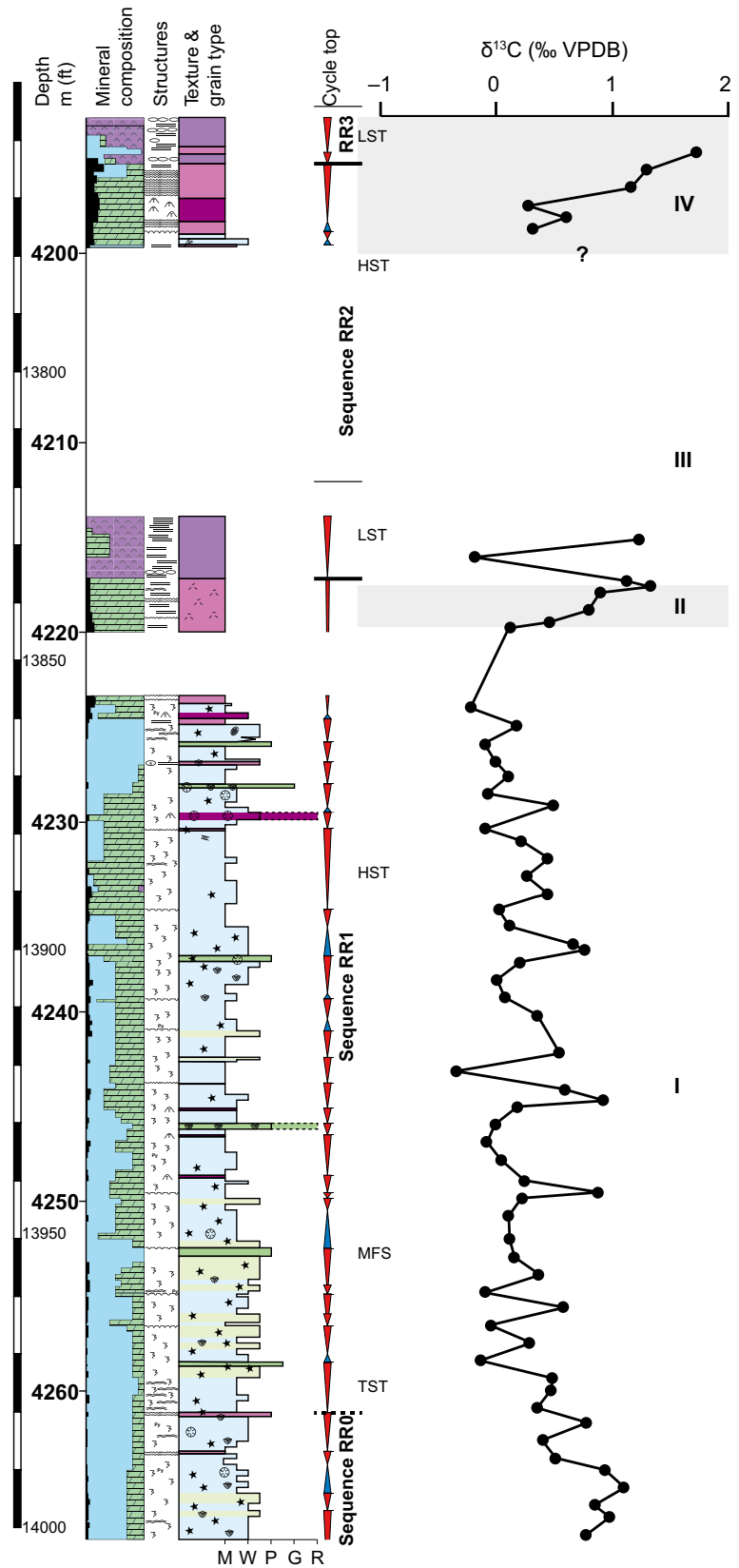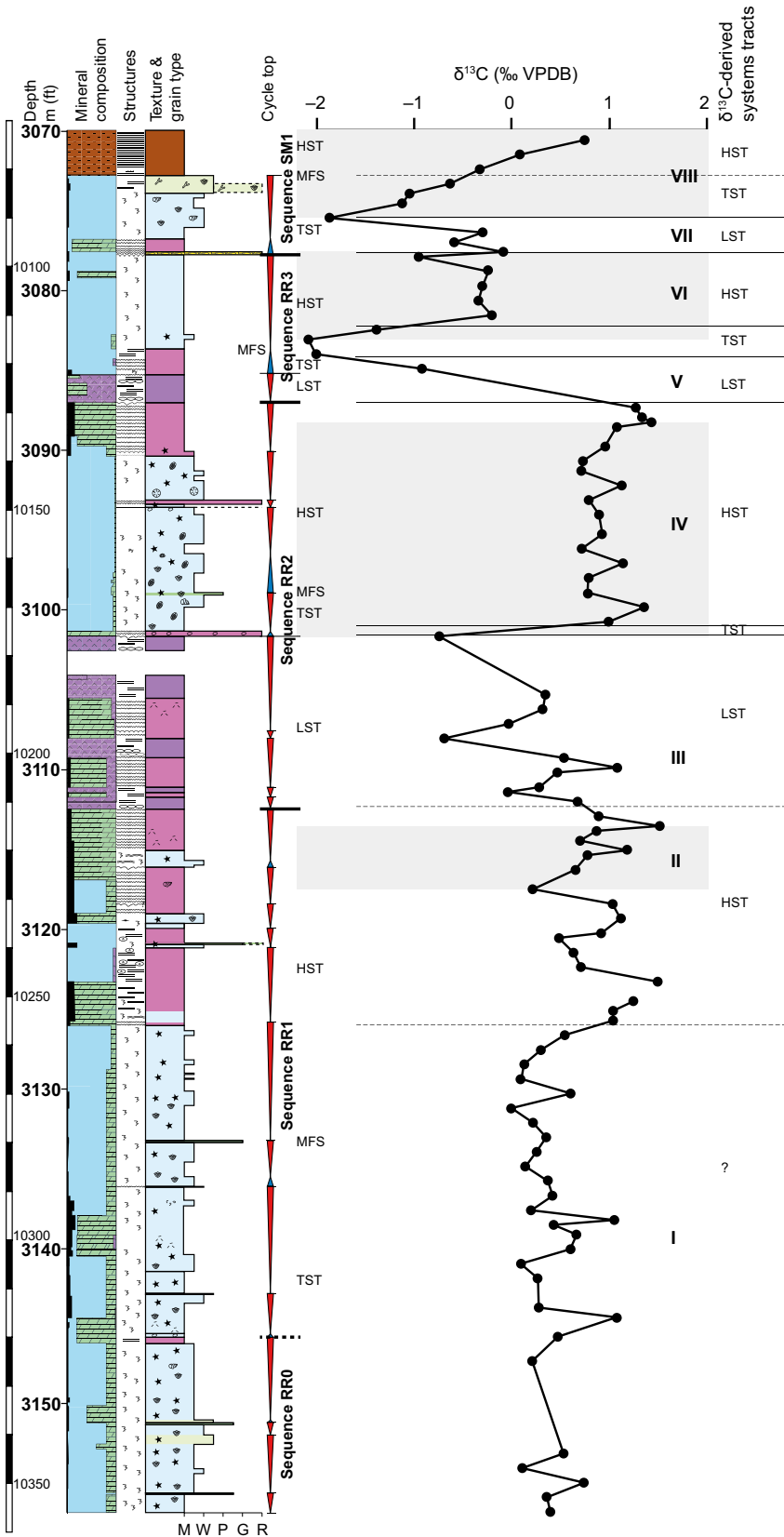
Fig. 6. Detailed stratigraphic column of core #8010 (Urlacher State #1, Hettinger County, North Dakota) showing mineral composition, sedimentary structures, Dunham rock types, parasequences and long-term depositional sequences. Upward-deepening units are shown by upward-narrowing triangles; upward-shallowing units are shown by upward-widening triangles. TST = transgressive systems tract, MFS = maximum flooding surface, HST = highstand systems tract, LST = lowstand systems tract. Carbon-isotope curve, carbon-isotope stages (Roman numerals), and δ¹³C-derived systems tracts are on the right side of the figure. For key to symbols, see Fig. 4. For well location, see Fig. 1.

Tidal-flat dolomite (Fig. 7A to D) makes up the bulk of the laminated members in the study area. This early diagenetic replacement dolomite replaces tidal-flat, microbial lithofacies and forms porous replacement mosaics of interlocking aphanocrystalline to finely crystalline dolomites (<1 to 30 μm). Individual crystals are anhedral to subhedral, relatively clear to slightly hazy without zonation. Lamination is best visible in polished cores, while in thin sections, it is vaguely discernible as fine alternation of millimetre-scale laminae with different dolomite crystal sizes. Cathodoluminescence imaging yields the dark orange to red colour of these dolomites.

Fine to medium crystalline (2.5 to 80 μm) dolomite replaces the burrow-fill lithofacies (mostly skeletal wackestone, less commonly packstone) of the burrowed members (Fig. 7E to H). The dolomitized burrows show relatively sharp burrow-matrix boundaries, resulting in a clear burrow-mottled fabric. Elsewhere, these boundaries are less sharp, exhibiting thin dolomitized haloes surrounding the burrows, with floating, isolated fine dolomite crystals decreasing in abundance from dolomitized burrows into the non-burrowed micrite matrix. These relatively 'dirty' crystals are subhedral to euhedral. These dolomites exhibit a dark orange to red cathodoluminescence colour similar to tidal flat dolomite. Locally, zoned crystals with dark, cloudy nuclei and clear rims are visible in plain polarized light. Under cathodoluminescence, these crystals show somewhat brighter rims and darker orange to red cores (Fig. 7F and H).

Other dolomite types are subordinate and comprise only a minor fraction of the entire dolomite succession. These include medium-grained dolomites that are associated mostly with stylolites, voids and minor fractures, and coarse-grained zoned euhedral dolomite that is rarely found in localized larger voids.

Carbon-isotope chemostratigraphy

In this paper, the stable carbon-isotope signal is split into stages to facilitate discussion and enable correlation with the North American carbon-isotope stratigraphy in the Richmondian Stage (Bergström *et al.*, 2010c). Stable carbon-isotope stages (Table 2) are identified based on positive excursions, shifts from positive to negative values and relatively uniform values. To avoid confusion with depositional sequences (0 to 3) and the production interval (D to A) terminology, the stable carbon-isotope stages are labelled with Roman numerals, and are described below for each of the cores used in this study.

Simpson #1 (#9800; Williams County)
Stage I represents an interval of relatively uniform to gently decreasing $\delta^{13}C$ values between 1.0‰ and −1.0‰ (Fig. 4). It is followed by a pronounced increase from −1 to +1‰ (stage II), while the overlying stage III shows stepwise decreasing values to −1‰. The subsequent stage IV is characterized by a stepwise increase in carbon-isotope values up to value of 2.1‰. Stage V is defined by a rapid decreasing trend towards $\delta^{13}C$ values near −2.5‰. During subsequent stage VI, the carbon-isotope values increase stepwise to 1.1‰; the increase is interrupted by a negative spike (−1.3 to −3.1‰) below the stage top. The overlying stage VII is characterized by a stepwise decrease towards $\delta^{13}C$ values near −2.8‰. In the topmost part of the section, the basal part of stage VIII exhibits an increase in carbon-isotope values to −0.9‰.

Federal #10-1 (#9103; Dunn County)
An interval of relatively uniform $\delta^{13}C$ values scattered from −0.4 to 1.1‰ characterizes stage I (Fig. 5). The overlying stage II shows a rapid increase from 0.1 to 1.1‰. The $\delta^{13}C$ value trends for stage III and the lower part of stage IV remain unknown due to lack of core material. The upper part of sampled stage IV is characterized by an increase in $\delta^{13}C$ values from 0.3 to 1.7‰; this is also the topmost cored interval through the Red River Formation from the Federal #10-1 well.

Figure 7. Paired plane light (left) and cathodoluminescent (right) photomicrographs of the main dolomite types of the Red River Formation. (A), (B), (C) and (D) Crinkly laminated dolomudstone (microbial dololaminite), B laminated member. Note the wispy dark laminae representing remains of organic matter forming microbial mats. The dolomite exhibits replacement mosaics composed of non-zoned, aphanocrystalline to finely crystalline non-planar and planar-s crystals exhibiting dark orange to red luminescence. (E), (F), (G) and (H) Finely to medium-grained planar-s dolomite replacing burrow fill in lime mudstone (E) and (F) and skeletal wackestone (G) and (H) matrix. Contact between burrow fill (b) and matrix (m) is marked by dashed lines. Note the similar dark orange to red cathodoluminescence colour of burrow fill as in tidal-flat dolomite, and non-luminescent to deep red micrite matrix.
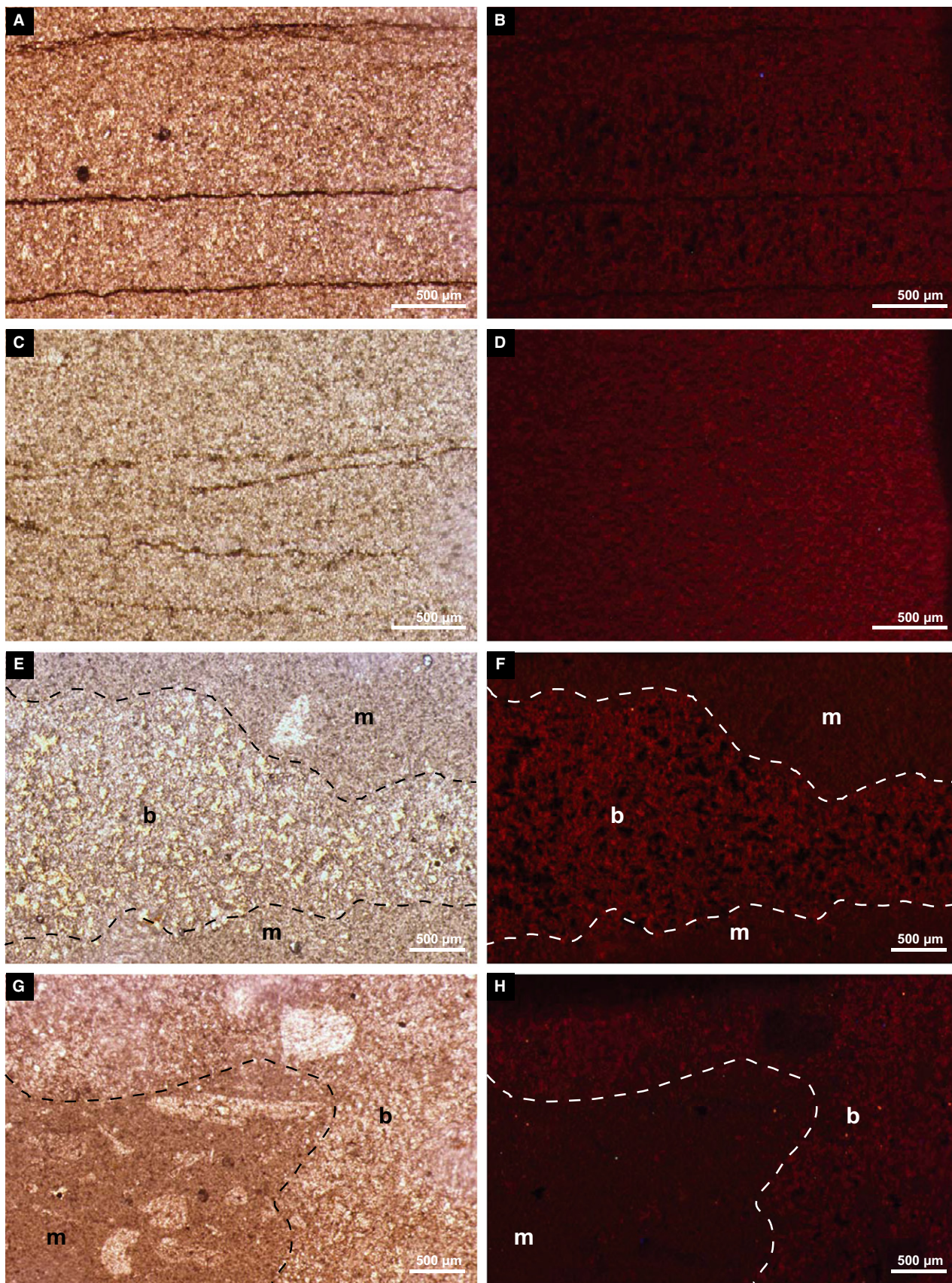
Table 2. Upper Katian carbon-isotope stages, Williston Basin, North Dakota, USA.

C-isotope stage	C-isotope trend	C-isotope shift amplitude (‰ VPDB)	Interval thickness (m)	Lithostratigraphic unit
VIII	Pronounced positive shift	2.7	>5	Red River Formation to Stony Mountain Formation transition
VII	Stepwise negative shift	1.8–3.9	2.1–8.1	Upper A interval
VI	Pronounced positive shift interrupted by a negative spike (up to 2‰) below the stage top	2–3.6	5.5–12	Lower A interval
V	Sharp negative shift	3.5–4.6	5.2–7	Uppermost B laminated member to lowermost A interval
IV	Pronounced positive shift	2.1–3.1	4–13.4	B burrowed member to B laminated member
III	Stepwise negative shift	2–2.2	10.7–11.9	Uppermost C laminated member to B burrowed member
II	Pronounced positive shift	0.8–2	2.1–6.4	Upper C laminated member
I	Relatively uniform values of between −1‰ and 1.5‰	–	>48	Upper C burrowed member to lower C laminated member

Urlacher State Unit #1 (#8010; Hettinger County)

An interval of relatively uniform $\delta^{13}C$ values between 0‰ and +1.5‰ characterizes stage I (Fig. 6). This trend is interrupted by a positive shift from 0‰ and +1.5‰ in the upper part of the stage; such a pronounced positive shift has not been identified in the other two cores. In the overlying stage II, the $\delta^{13}C$ values increase up-section from 0 to +1.5‰, while stage III shows stepwise decreasing values to −0.7‰. Stage IV begins with a sharp increase to *ca* +1.4‰, followed by a sequence of relatively uniform values of between +0.7 and +1.1‰ and a peak of 1.4‰ at the top. Stage V is characterized by a rapid decrease to −2.1‰, the lowest $\delta^{13}C$ value recorded from the Simpson #1 core. An increase towards −0.1‰, interrupted by a negative spike (−0.2 to −1‰) below the top characterizes stage VI. During subsequent stage VII, carbon-isotope values decrease to −1.9‰. In the overlying stage VIII, carbon-isotope values continuously increase, reaching the maximum value of +0.8‰ at the very top of the sampled interval, which is in the lowermost part of the Stony Mountain Formation.

Stable oxygen isotopes

Stable oxygen-isotope values of limestone range between −8.0‰ VPDB and −3.8‰ VPDB, and between −6.8‰ VPDB and −3.9‰ VPDB in dolomite (Fig. 8). The mean $\delta^{18}O$ value for limestone is −6.1‰ VPDB. The mean value for oxygen isotopes of dolomite whole rock samples is −4.9‰ VPDB, i.e. on average dolomites are 1.2‰ heavier than limestones. The modern dolomite and calcite forming beneath the sabkhas of the United Arab Emirates have an equilibrium fractionation factor ($\Delta\delta^{18}O_{dol-cal}$) of 3.2‰ VPDB at *ca* 35°C (McKenzie, 1981). Vasconcelos *et al.* (2005) proposed a slightly lower $\Delta\delta^{18}O_{dol-cal}$ value of 2.6‰ for dolomite and calcite that formed from isotopically similar fluids at similar temperatures. Thus, a small positive shift in oxygen-isotope values between dolomite and limestone suggests that the dolomites picked up lighter signature due to burial at great depth (3 to 4 km). The effects of late burial diagenetic alteration are also suggested by significantly lower values than Ordovician oxygen-isotope values based on valid marine proxies (translucent fibrous calcite, marine equant calcite and bladed calcite) which range between −5.8‰ VPDB and −2.5‰ VPDB (Tobin & Walker, 1997). Consequently, the oxygen-isotope values are not used and discussed in the present paper to facilitate correlation between the studied wells, or to evaluate the Late Ordovician sea water values.
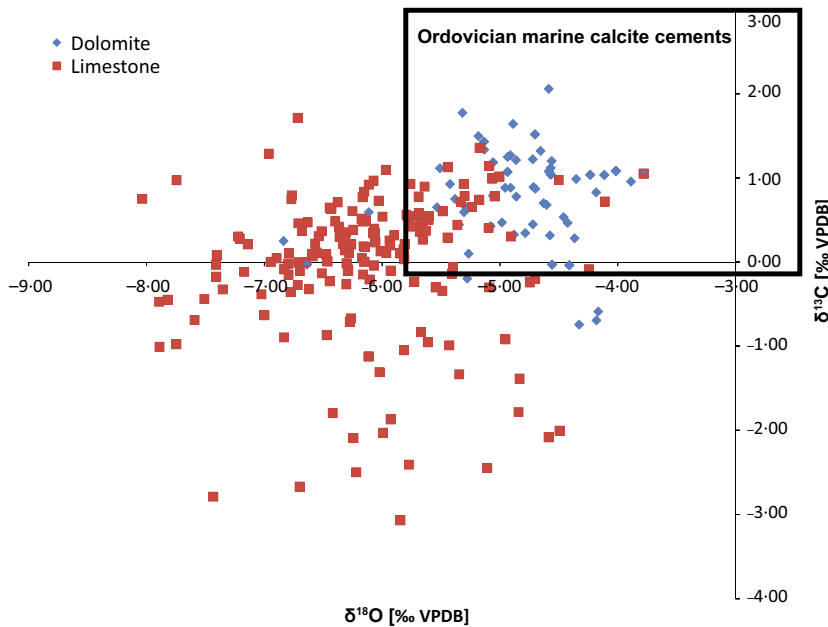
Fig. 8. Carbon and oxygen isotopic composition for samples from all three sampled cores. The black rectangle marks values of Ordovician marine calcite cements from Tobin & Walker (1997).

INTERPRETATION AND DISCUSSION

The potential effect of local environmental changes on stable carbon-isotope values

Carbon-isotope values of shallow-marine carbonate sediments are influenced by a number of effects, including taxonomic variation, diagenesis, carbonate mineralogy, as well as taphonomic processes, and thus should be used cautiously and in combination with additional sedimentological and palaeontological data for stratigraphic interpretations (Gischler *et al.*, 2009; Oehlert *et al.*, 2012). Use of the $\delta^{13}C$ record for correlation purposes presumes that these values retain the original sea water $\delta^{13}C$ value recorded from an isotopically homogenous portion of the ocean that is consistent between basins (e.g. Panchuk *et al.*, 2005, 2006; Swart & Kennedy, 2012). Due to rapid mixing of carbon within the atmosphere and the ocean surface layer, and due to exchange between these two carbon reservoirs, a change in carbon cycle affects the $\delta^{13}C$ composition of dissolved inorganic carbon (DIC) in the pelagic surface ocean, which is in turn reflected in $\delta^{13}C$ values of pelagic carbonates precipitated from the sea water (Panchuk *et al.*, 2005). An increase in $\delta^{13}C$ typically results from an increased production and/or burial of organic matter, while a decrease reflects increased oxidation of organic matter and less organic carbon burial (e.g. Veizer & Hoefs, 1976; Schidlowski, 1979; Shackleton & Pisias, 1985; Oehlert *et al.*,

2012). The Ordovician marine $\delta^{13}C$ record can be obtained from the bulk carbonate matrix, calcite cement or larger skeletal organisms (for example, brachiopods). However, the studies of modern shallow-marine carbonates have shown that their $\delta^{13}C$ signature can be very different from, and show no relation with, the variations in the $\delta^{13}C$ values of the DIC in the oceans; the platform $\delta^{13}C$ record may be either drastically depleted (for example, Florida Bay: Loyd, 1964; Patterson & Walter, 1994) or enriched (for example, the Bahamas: Swart & Eberli, 2005; Swart *et al.*, 2009) with respect to their pelagic equivalents. The variations in $\delta^{13}C$ profiles have also been described for Ordovician epeiric sea carbonates from different locations (e.g. Ludvigson *et al.*, 1996, 2004; Patzkowsky *et al.*, 1997; Panchuk *et al.*, 2005, 2006; Immenhauser *et al.*, 2008; Ainsaar *et al.*, 2010). These geographical variations in the $\delta^{13}C$ geochemical signature of epeiric carbonates often reflect restricted sea water circulation in combination with local environmental influences (e.g. Panchuk *et al.*, 2005, 2006; Oehlert *et al.*, 2012). Similar to lacustrine carbonates, the negative values of $\delta^{13}C$ of epeiric sea carbonates may result from water inflow containing dissolved CO_2 from older rocks, or from respiration processes or hydrosphere to atmosphere CO_2 exchange; enrichment in $\delta^{13}C$ may indicate photosynthesis during increased basin closure and long water residence time (Sarg *et al.*, 2013). Given that the Williston Basin was periodically isolated from

the open ocean, it is possible that the carbonates that precipitated from such a large body of restricted water mass have unique, inherently different isotopic composition from that of the open ocean (Swart & Eberli, 2005).

It is generally accepted that photosynthetic processes increase the $\delta^{13}C$ value of skeletal carbonate precipitated by different organisms (e.g. Cummings & McCarthy, 1982; Swart, 1983; McConnaughey, 1989; Swart *et al.*, 2009). In Williston Basin, the highest $\delta^{13}C$ values characterize tidal-flat dololaminites (C and B laminated members below regional anhydrites; Figs 4 to 6). These laminites formed during the late sea-level highstand, when aggradation along the basin margins resulted in basin restriction, long water residence time and subsequent progradation of tidal flats across the basin. Efficient photosynthetic activity by flourishing cyanobacteria could have enriched surface water with respect to ^{13}C, which then was incorporated in the inorganic carbonate (cf. Sarg *et al.*, 2013), and resulted in positive excursions in $\delta^{13}C$ values recorded in top C and B laminite members.

The $\delta^{13}C$ values of marine algal carbonate reflect phylogenetic and ontogenetic changes in photosynthesis that are reflected in the $\delta^{13}C$ value of the calcifying fluid due to modification of the photosynthesis/respiration ratio (Lee & Carpenter, 2001). The calcareous green algae are abundant within the C and B burrowed members of the Red River Formation, the latter with Codiacean *Dimorphosiphon* being the major carbonate sediment producer (Rendall & Husinec, 2012). The $\delta^{13}C$ values from the three studied sections vary between −0.3‰ and +1.1‰ for the C burrowed member and between −0.8‰ and +1.2‰ for the B burrowed member (Figs 4 to 6), and are overall heavier than the mostly negative values recorded from the coeval successions of the Cincinnati region, USA (Fig. 9). This suggests that the significant carbonate production by Codiaceans could have affected the $\delta^{13}C$ values of the Williston Basin, and resulted in isotopically slightly enriched DIC compared with the coeval bryomol-dominated, temperate-water carbonate intervals from the mid-continent, the latter are also affected by an enhanced influx of dissolved organic carbon with low $\delta^{13}C$ values from rivers and coastal wetlands along the Transcontinental Arch (Panchuk *et al.*, 2006).
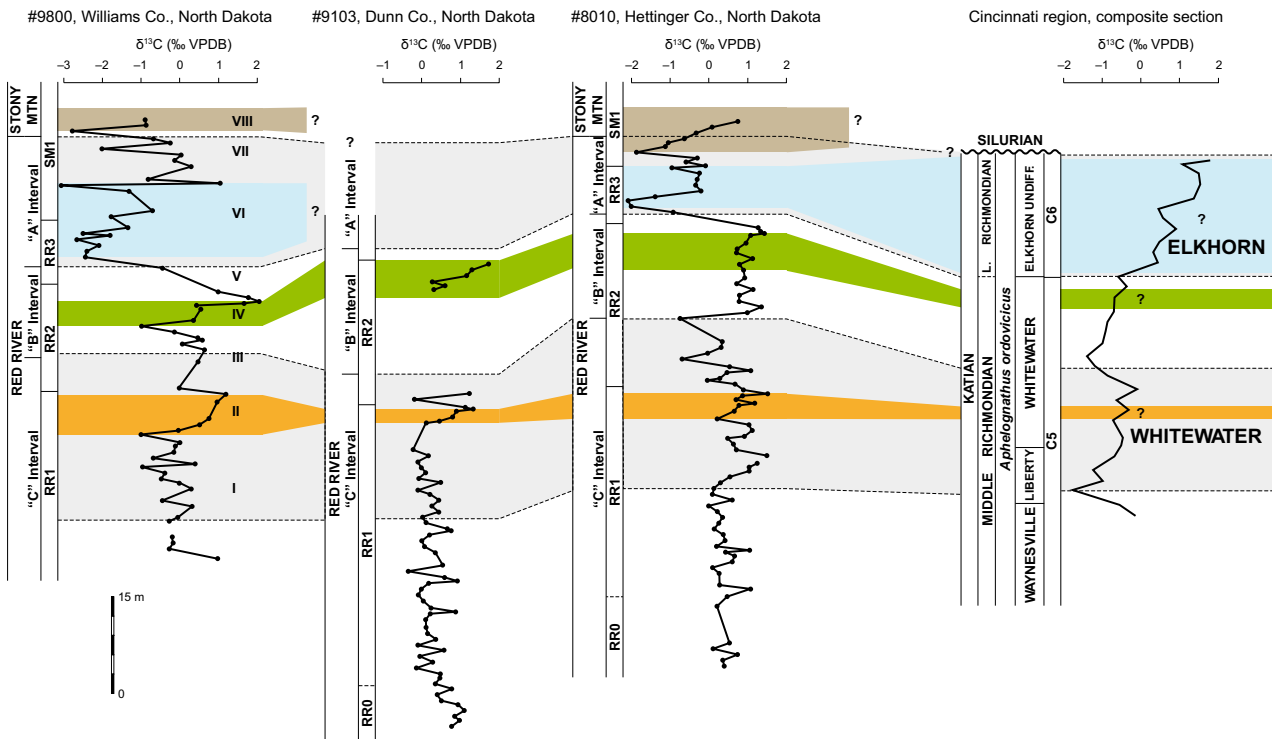

Fig. 9. Correlation of carbon-isotope curves of studied Red River cores and proposed correlation with Cincinnati region. Roman letters indicate carbon-isotope stages identified in this study. Cincinnati positive $\delta^{13}C$ excursions (Bergström *et al.*, 2007, 2010d) are on the right side of figure.

Diagenetic overprints

Petrographic evidence from the sampled laminated and burrowed Red River members, including fine crystal size and lack of zoning, suggests an early, replacive origin for the bulk of the dolomite. Medium-grained dolomites that are associated mostly with stylolites, voids and micro-fractures are late diagenetic and formed after burial at medium depths, probably between 500 m and 1500 m (cf. Machel, 1999; Mountjoy et al., 1999). The dolomitization is thorough in the laminated members and decreases downwards in the burrowed members, away from the anhydrite members. This suggests that a reflux of dense hypersaline brines associated with evaporative drawdown lead to a penecontemporaneous replacement of mud in tidal flats and porous burrows of the underlying burrowed limestone by finely crystalline dolomite. The early, replacive dolomitization of the tidal flat facies resulted in abundant intercrystalline porosity of the Red River laminated members. This initial porosity and permeability have been well-preserved and suggest that the tidal flat facies has not been extensively modified by burial dolomitizing fluids that would have transformed porous and permeable early diagenetic dolomites into non-porous dolomite mosaics of tightly interlocking crystals (cf. Montanez, 1997). Porous intervals are isolated stratigraphically from one another by impermeable anhydrite beds that also acted as permeability barriers to dolomitization. Anhydrite laths and needles also occur in the underlying porous sediments. In the samples studied, there is no evidence of dolomite replacing these minerals, which further suggests that the system must have been effectively sealed by the evaporites that prevented the excessive fluid flow needed for extensive burial dolomitization (cf. Melim & Scholle, 2002). Thus, the vertical stacking of the Red River units produced a stratified three-dimensional network with three major aquitards (anhydrite members) bracketing fluid flow conduits (burrowed and laminated members).

Cathodoluminescence evidence suggests a similar dolomitization history for both sampled burrowed and laminated dolomite. The dark orange to red luminescence colour of these dolomites under the operating conditions suggests the presence of Mn^{2+} and Fe^{3+} in the burial fluids, although many other elements can also potentially serve as activators and quenchers of CL in carbonates (e.g. Machel & Burton, 1991).

The Mn^{2+} and Fe^{3+} can substitute Ca^{2+} in the carbonate lattice, but are mobile only under reducing conditions (Garrels & Christ, 1965). Thus, they are suggestive of diagenetic stabilization within a burial diagenetic environment, or reducing conditions associated with bacterial sulphate reduction in microbial mats (cf. Banner et al., 1988; Moore et al., 1988); the latter is suggested by the local presence of disseminated pyrite in tidal flat facies (cf. Montanez & Read, 1992). The uniform, non-patchy luminescence of both laminated and burrow-fill dolomite might also suggest their early diagenetic origin (cf. Tobin & Walker, 1997).

Carbon-isotope values from valid Ordovician marine proxies appear to range between 0‰ VPDB to 3‰ VPDB (Tobin & Walker, 1997). The range in the $\delta^{13}C$ composition of the Red River limestone and dolomite is slightly greater (−3.0‰ VPDB to 2.1‰ VPDB) which could reflect diagenetic alteration (e.g. Allan & Matthews, 1977; Lohmann, 1988; Immenhauser et al., 2003; Swart & Eberli, 2005). It is important to stress that both dolomite and limestone from the study area have similar $\delta^{13}C$ values (Fig. 8), suggesting that carbon was rock buffered, and thus apparently could represent the original marine $\delta^{13}C$ record. In addition, the range of the Red River $\delta^{13}C$ values is within the 5‰ range of modern pore water variation (Patterson & Walter, 1994), and thus requires no input of external sources of carbon (cf. Melim & Scholle, 2002). The values extending into the lower left quadrant (Fig. 8) probably have been reset either by early diagenetic bacterially mediated sulphate reduction (cf. Sass et al., 1991; Chafetz et al., 1999), or by late burial fluids, including input of depleted carbon from hydrocarbons (Anderson & Arthur, 1983). There are several shifts to low $\delta^{13}C$ values that exceed 2.0‰ VPDB between vertically adjacent samples (Figs 4 to 6). Such shifts to negative values are common both in ancient limestone and dolomite (e.g. Curtis et al., 1972; Kaufman et al., 1993; Vahrenkamp & Swart, 1994; Chafetz et al., 1999; Railsback et al., 2003), where they presumably occur due to either diagenesis associated with descent of meteoric water beneath a soil horizon and subsequent interaction with the host carbonate strata, or diagenesis associated with bacterially mediated sulphate reduction of extensive microbial mats in sabkha-type dolomites (Chafetz et al., 1999). However, typical negative shifts in modern carbonates associated with subaerial exposure are much greater (6 to

8‰ VPDB; Allan & Matthews, 1977, 1982) than those from the studied succession. Similar to the Triassic Latemar platform in the Dolomites (Christ *et al.*, 2012), it is very likely that meteoric diagenesis is not responsible for negative shifts in $\delta^{13}C$ values of the Red River Formation, as neither evidence for the existence of soils nor evidence to associated negative $\delta^{13}C$ shifts to subaerial exposure has been recognized in the studied cores. The abundant evaporites also imply an arid and warm climate not supportive of vegetation cover that could have supplied depleted carbon isotopes from soil to the underlying carbonates. Furthermore, the overall $\delta^{13}C$ values for laminated dolomite are higher than those from the overlying anhydrites (from which thin dolomitic interbeds were sampled) (Figs 4 to 6), suggesting that following dolomitization, the tidal-flat laminite probably was not subjected to extensive diagenesis in contact with meteoric waters.

Some of the pronounced (>2‰ VPDB) negative excursions occur near hardgrounds or pyritic crusts, and could be related to bacterial sulphate reduction either within benthic euxinic waters or in shallow-marine phreatic pore fluids at the sediment–water interface (Swart & Melim, 2000; Ludvigson *et al.*, 2004; Dickson *et al.*, 2008; McLaughlin *et al.*, 2011). The negative excursions occur at the boundaries between $\delta^{13}C$ segments VI to VII and VII to VIII in well #9800 (Fig. 4), and at the base of the A interval (within C-segment V) in well #8010 (Fig. 6). These excursions suggest that some of the negative spikes could be related to (or possibly accentuated by) local flooding events accompanied by euxinic waters, and thus do not reflect the contemporaneous oceanic carbon-isotope signal (cf. Ludvigson *et al.*, 2004). However, both hardgrounds and pyritic crusts are relatively abundant within the studied succession, and most of them do not show significant negative excursions on the $\delta^{13}C$ curve. This may also be a remnant of a relatively spaced sampling interval (3 ft or *ca* 90 cm); much denser sampling around these intervals would yield a more detailed $\delta^{13}C$ signal and probably more clues to their driving mechanism.

To summarize, petrographic and cathodoluminescence evidence, coupled with a stable isotope record, suggests an early diagenetic origin of the sampled dolomite, with diagenetic stabilization under non-oxidizing conditions and the presence of isotopically more negative burial fluids, probably prior to burial at medium depths. The lack of major burial overprint and porosity-occluding overdolomitization (Morrow, 1982; Lucia & Major, 1994) could have been caused by the presence of thick anhydrites that acted as permeability barriers to vertical flow of burial fluids. This flow may also have been impeded by abundant bedding-parallel stylolites and dissolution seams, similar to the major Lower Cretaceous reservoirs of the United Arab Emirates where the lower porosity and permeability values are found associated with the well-developed stylolites (Alsharhan & Sadd, 2000).

Intrabasinal correlation

The three middle to upper Richmondian sections from North Dakota exhibit several similarities in the stratigraphic position and magnitude of $\delta^{13}C$ stages (Fig. 9). All of these sections show the highest $\delta^{13}C$ values in C and B laminated members, and two of the three studied sections exhibit minimum values in the A interval (the A interval from section #9103 has not been cored). Relative uniformity or a gentle decrease in stable carbon-isotope values characterizes $\delta^{13}C$ stage I that corresponds to the upper C burrowed and the lower C laminated members. Three minor positive $\delta^{13}C$ excursions can be identified, from oldest to youngest: (i) $\delta^{13}C$ stage II is registered in all three cores within the upper C laminated member; (ii) $\delta^{13}C$ stage IV is also registered in all three cores. Its stratigraphic span varies slightly (upper B burrowed to B laminated in #9800, B burrowed to B laminated in #8010, incomplete record for #9103), but the peak is within the B laminated member; and (iii) $\delta^{13}C$ stage VI is registered within the lower part of the A interval in cores #9800 and #8010; no core was available from well #9103. These positive excursions could be related to local oceanographic conditions within the Williston Basin epeiric sea, presumably reflecting one or more processes, including increased organic productivity, increased organic carbon sequestration, changes in relative abundance of different components in organic matter, or enhanced preservation of organic carbon caused by marine anoxia (e.g. Weissert, 1989; Derry *et al.*, 1992; Brasier *et al.*, 1994; Calvert *et al.*, 1996; Glumac & Walker, 1998; Jenkyns *et al.*, 2002); they also may represent regional events across the Late Ordovician western passive continental margin of North America, and are potentially useful for correlation.

Extrabasinal correlation

The Late Ordovician is characterized by two major shifts to positive $\delta^{13}C$ values; the early Katian Guttenberg and the Hirnantian excursions. In North America, the Guttenberg excursion ranges from the uppermost *Phragmodus undatus* Midcontinent Conodont Zone to near the top of the *Plectodina tenuis* Midcontinent Conodont Zone. Its cause of formation is still enigmatic (Bergström *et al.*, 2010c, 2014). The Hirnantian excursion begins in the topmost *Paraorthograptus pacificus* graptolite Zone (top of *Amorphognathus ordovicicus* Conodont Zone) and ends in the lower *Normalograptus persculptus* Graptolite Zone (Bergström *et al.*, 2010c, and references therein). The Hirnantian positive shift most probably reflects an enhanced ocean circulation that increased productivity and sequestration of organic carbon (Brenchley *et al.*, 1994), or increased weathering of carbonates during eustatically driven sea-level fall (Kump *et al.*, 1999). Besides the Guttenberg and the Hirnantian, five positive $\delta^{13}C$ excursions have been identified in the Upper Ordovician between the Guttenberg and the Hirnantian excursions (Ainsaar *et al.*, 2004, 2010; Kaljo *et al.*, 2004; Bergström *et al.*, 2007, 2010a).

In North America, Bergström *et al.* (2007, 2010d) recognized the following positive $\delta^{13}C$ excursions, from oldest to youngest: Kope (upper *Diplocanthograptus spiniferus* to *Geniculograptus pygmaeus* Graptolite Zones; substantial part of *Belodina confluens* Conodont Zone), Fairview (poorly controlled by graptolites, excursion near the base of *Amplexograptus manitolinensis* Graptolite Zone; mostly within upper part of *Oulodus velicuspis* Conodont Zone); Waynesville (upper part of *Amplexograptus manitolinensis* Graptolite Zone; lower part of *Amorphognathus ordovicicus* Conodont Zone), Whitewater (within *Dicellograptus complanatus* Graptolite Zone; upper, but not uppermost, part of *Amorphognathus ordovicicus* Conodont Zone) and Elkhorn (upper *Amorphognathus ordovicicus* Conodont Zone).

If variations in stable carbon-isotope profiles from the Williston Basin reflect variations in the original marine $\delta^{13}C$ values, then they should be correlatable with previously published $\delta^{13}C$ profiles from coeval strata of Midcontinent USA (Bergström *et al.*, 2007, 2010d) that were shown to co-vary with coeval $\delta^{13}C$ profiles from the East Baltic region (Ainsaar *et al.*, 2004, 2010; Kaljo *et al.*, 2004). Based on the $\delta^{13}C$ analysis coupled with the available biostratigraphic data, a Williston Basin to Midcontinent Cincinnati Region correlation is presented in Fig. 9. Besides method-inherent caveats, for example, different sampling densities or different trends in thicknesses, the correlation may be further impeded by the fact that the Cincinnatian Series curve represents a composite curve (Bergström *et al.*, 2010a).

The oldest three positive $\delta^{13}C$ excursions from the Cincinnati Region (Kope, Fairview and Waynesville) are not recorded within the upper Red River Formation. This is in agreement with the conodont and brachiopod evidence, and further suggests that the upper Red River Formation is stratigraphically younger than the upper part of *Amplexograptus manitolinensis* Graptolite Zone (lower part of *Amorphognathus ordovicicus* Conodont Zone); i.e. it is late Katian in age. The upper part of the Cincinnati $\delta^{13}C$ curve shows an overall gradual positive trend (-2 to $+2‰$ VPDB) with two major excursions to positive values (Whitewater and Elkhorn), which is different from an overall gradually negative trend (*ca* $+1‰$ to *ca* $-2‰$ VPDB) in the Williston Basin. The positive $\delta^{13}C$ shift within the upper C laminated member of the Red River Formation ($\delta^{13}C$ stage II) is interpreted to correspond to a minor shift to positive values (*ca* $0.5‰$ VPDB) within the Whitewater $\delta^{13}C$ excursion from the Cincinnati Region, but the absolute $\delta^{13}C$ values from the Williston Basin are *ca* $1.5‰$ higher, and are more similar to those from coeval Moe excursion in Estonia (Ainsaar *et al.*, 2004, 2010; Kaljo *et al.*, 2004, 2008). The curve segment in the Red River B interval ($\delta^{13}C$ stage IV), with most values between $0‰$ and *ca* $1‰$ and the heaviest $\delta^{13}C$ value of *ca* $+2‰$ VPDB (well #9800), shows no corresponding excursion in the Cincinnati region, and can only be biostratigraphically correlated with a minor wiggle in the curve segment of the upper Whitewater Formation between the Whitewater and Elkhorn excursions in the Cincinnati curve (Fig. 9). The youngest Ordovician excursion in the Cincinnati Region (Elkhorn excursion, *sensu* Bergström *et al.*, 2010d) shows a significant *ca* $3‰$ shift to positive values in that area. Excluding the core #9103, the $\delta^{13}C$ excursion in the A interval ($\delta^{13}C$ stage VI), which starts a little above the base of sequence RR3 in the Williston Basin cores #9800 and #8010, shows a pronounced excursion to negative values below its base ($\delta^{13}C$ stage V) which is not present in the Cincinnati curve. The $\delta^{13}C$ stage VI appears to correspond to the

overall positive trend of the Cincinnati δ^{13}C curve (Elkhorn excursion), but the former is much more complex and contains a major excursion to negative values (core #9800) that is not present in the Cincinnati curve. The remainder of the Williston Basin δ^{13}C curve covers a stratigraphic interval that is not preserved in the Cincinnati Region and represents the first published δ^{13}C values from the Stony Mountain Formation. No isotope data are yet known from higher parts of the Stony Mountain Formation, but Demski *et al.* (2011) recognized the Hirnantian excursion in the Stonewall Formation of Manitoba, indicating the presence of Hirnantian strata in the margin of the Williston Basin. Finally, given the different overall trend and absolute δ^{13}C values between the Williston Basin and the Cincinnati Region, it seems likely that correlation based on δ^{13}C records would not have been possible without a solid middle–upper Richmondian biostratigraphic foundation. The differences in the δ^{13}C overall trend and absolute values may be suggestive of a lack of exchange between waters of the Williston Basin and the Midcontinent (Rendall & Husinec, 2012, and references therein), as well as the influence of different regional environmental processes or diagenetic histories discussed in the preceding sections.

One of the thickest and most studied upper Katian and Hirnantian successions in North America, with detailed δ^{13}C chemostratigraphy, is that on Anticosti Island in Québec. Here, *ca* 360 m of the more than 1 km thick Upper Ordovician succession of dominantly richly fossiliferous carbonate rocks is exposed well in numerous sections (e.g. Twenhofel, 1929; Lespérance, 1982; Copper, 2001). The topmost 60 to 70 m of this remarkable sequence is classified as the Ellis Bay Formation and the underlying, *ca* 950 m thick, mostly unexposed, succession is referred to as the Vauréal Formation (Fig. 10), the basal part of which contains graptolites of the *Pleurograptus linearis* and *Dicellograptus complanatus* zones (Riva, 1969). This indicates that most of the Vauréal Formation, as well as most of the Ellis Bay Formation, belongs to Stage Slice Ka4 of Bergström *et al.* (2009). The most detailed biostratigraphy of this succession is based on chitinozoans (e.g. Achab, 1977; Achab *et al.*, 2011) and conodonts (e.g. McCracken & Barnes, 1981; Nowlan & Barnes, 1981).

A summary of regional correlations of the Williston Basin, Anticosti Island and Latvian successions based on biostratigraphy and carbon-isotope chemostratigraphy is presented in Fig. 11. The δ^{13}C chemostratigraphy of the Katian succession on Anticosti Island has been investigated by several authors (e.g. Underwood *et al.*, 1997; Young *et al.*, 2010; Jones *et al.*, 2011). For a comparison with the Williston Basin succession, the present study uses the δ^{13}C values published by Young *et al.* (2010) because they cover the entire exposed part of the Vauréal Formation as well as the whole Ellis Bay Formation (Figs 10 and 11).

As shown in Fig. 10, the δ^{13}C values from the exposed Vauréal succession vary between −0.7‰ and near +1‰. Beginning in the middle part of the Homard Member, there is a notable increase in δ^{13}C values from baseline values between −1‰ and 0‰ to values *ca* +0.5‰. With minor variation, values of this magnitude persist to the upper Joseph Point Member–lower Mill Bay Member, where there is a decline that culminates in values as low as *ca* +0.5‰. This curve segment with elevated values, which covers a *ca* 120 m thick succession, has the biostratigraphic position of the Elkhorn excursion in the Cincinnati region, where it is located between the Hirnantian and the Whitewater excursion (Bergström *et al.*, 2009). Compared with the excursion in the Red River Formation identified as the Elkhorn excursion, the excursion in the Vauréal Formation has more uniform δ^{13}C values, and does not show a negative spike recorded in core #9800 from the Williston Basin. The Anticosti Island values vary between 0‰ and *ca* +1‰, whereas those in the Red River Formation range from *ca* −3‰ to +1‰. The lowermost 50 m of the Vauréal curve shows slightly elevated δ^{13}C values, but further studies are needed to clarify whether this curve segment corresponds to the end of the Whitewater excursion identified in the Red River Formation, as suggested by its stratigraphic position in Fig. 10. The present authors expect that a complete representation of the Whitewater excursion is present in the subsurface portion of the Vauréal Formation, the isotope chemostratigraphy of which remains unstudied.

In a regional review, Bergström *et al.* (2010d) showed that the carbon-isotope excursions recognized in the Cincinnati region could be correlated with excursions occupying the same, or very similar, stratigraphic intervals in Baltoscandia. For instance, the Whitewater excursion, which occupies an interval around the *Dicellograptus complanatus* Zone in the Cincinnati region (cf. Goldman & Bergström, 1997), corresponds to the Baltoscandic Moe excursion, which is located in the lower Jonstorp Forma-
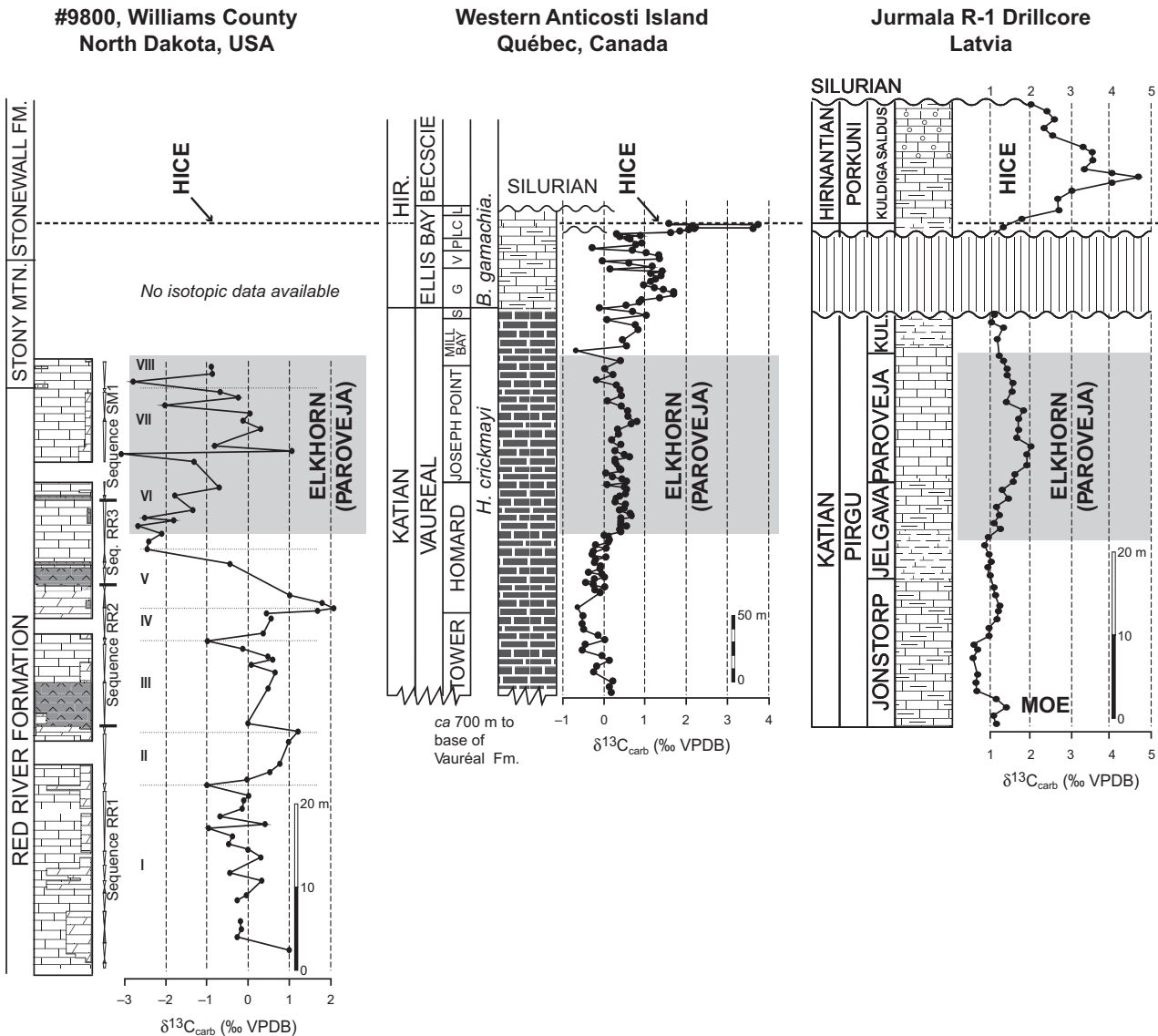
Fig. 10. Comparison of the δ¹³C chemostratigraphy in the Simpson #1 (#9800) well, Williams County, Williston Basin, that of the composite succession of the Vauréal and Ellis Bay formations on western Anticosti Island (after Young *et al.*, 2010), and that of the succession in the Jurmala R-1 well in Latvia (after Ainsaar *et al.*, 2010). Note the correlation of the Elkhorn and Paroveja excursions with that in the upper Red River Formation of the Simpson #1 well. The reference level for the alignment of the successions is the base of the Hirnantian excursion. No isotope data are yet available from most of the Stony Mountain and Stonewall formations, although the Hirnantian excursion has recently been recorded from the middle part of the Stonewall Formation. This correlation among the three successions is in good agreement with the biostratigraphy based on conodonts and shelly fossils.

tion in an interval that in Sweden has yielded graptolites of the same graptolite zone (Skoglund, 1963). In some East Baltic successions, there is an excursion between the Hirnantian and the Moe excursions that recently was renamed the Parojeva excursion (Ainsaar *et al.*, 2010). One of the most representative successions showing this excursion is the Jurmala R-1 drillcore from Latvia (Ainsaar *et al.*, 2010),

which is illustrated in Fig. 10, where it is compared with the Elkhorn excursion in the Anticosti Island and the Williston Basin successions. As shown by the different thickness figures, the Latvian succession is much thinner than the two others, and hence this excursion occupies a much more limited interval than on Anticosti Island and in the Williston Basin. It should also be noted that the Latvian δ¹³C curve lacks the
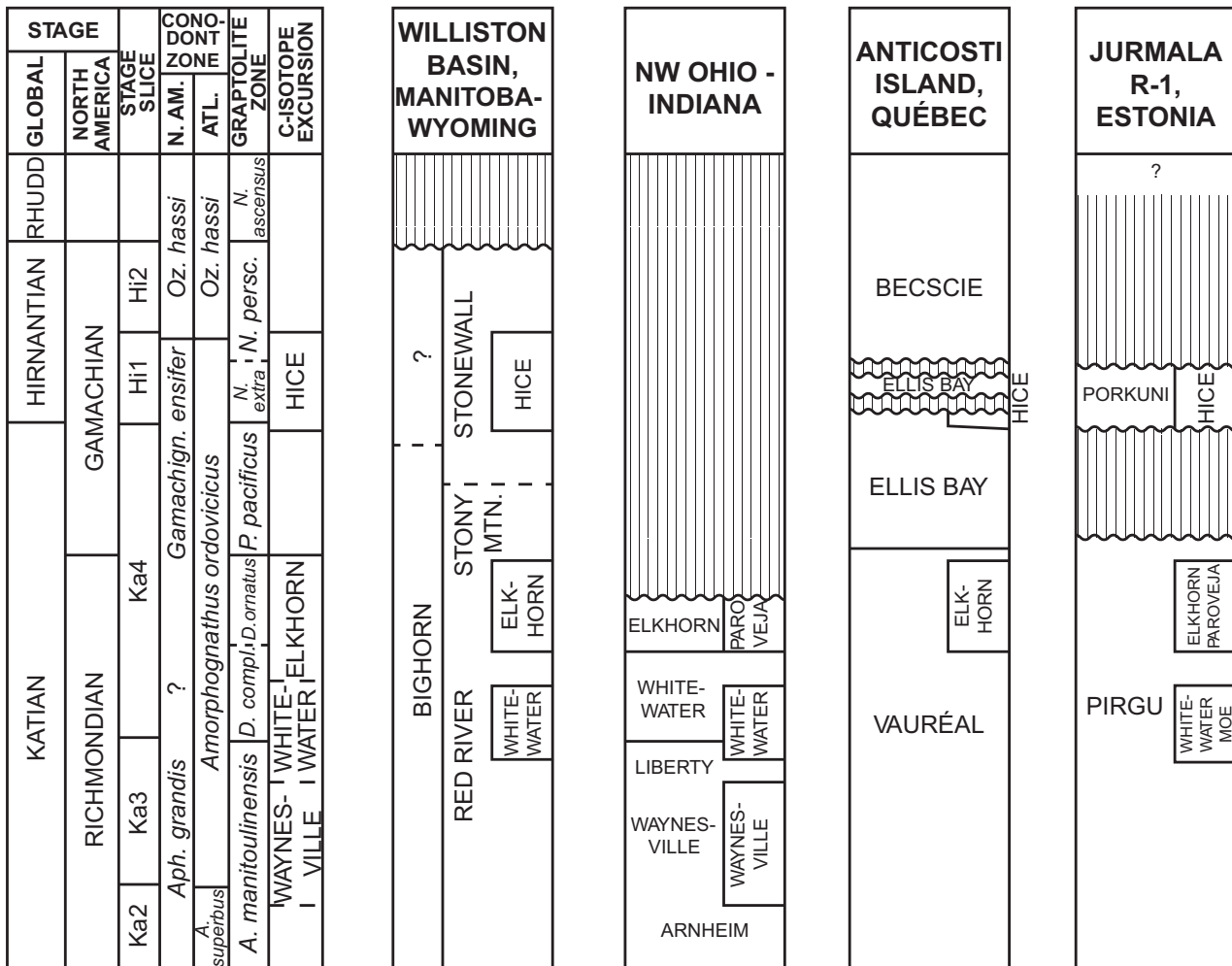
Fig. 11. Summary diagram showing the proposed correlation between the study successions based on biostratigraphy and δ¹³C chemostratigraphy. Vertical ruling indicates stratigraphic gaps. The North American upper Katian Conodont Zone succession is still unsettled, in that the Williston Basin *Aphelognathus divaricatus* and *A. shatzeri* zones and the Anticosti Island *Gamachignathus ensifer* Zone appear to cover a broadly similar stratigraphic interval. Note that based on its stratigraphic position in Ohio-Indiana, the Waynesville δ¹³C excursion is likely to be present in the lower Red River Formation as well as in the subsurface part of the Vauréal Formation. Abbreviations: *Aph., Aphelognathus*; *Gamachign., Gamachignathus*; *Oz., Ozarkodina*; N.Am., North America; Atl., Atlantic; *A. superbus, Amorphognathus superbus*; *D. compl., Dicellograptus complanatus*; *D. ornatus. Dicellograptus ornatus*; *P. pacificus, Paraorthograptus pacificus*; *N. extra., Normalograptus extraordinarius*; *N. persc., Normalograptus persculptus*; *N. ascensus, Normalograptus ascensus*.

characteristic noisy segment present in the uppermost Katian in the Anticosti Island curve. It is well-known that there is a more or less prominent stratigraphic gap in many Baltoscandian successions below the base of the Hirnantian (e.g. Lashkov & Paškevicius, 1989; Ainsaar *et al.*, 2010) and the appearance of the Jurmala R-1 isotope curve suggests the presence of a stratigraphic gap in that position, even if the succession in this drillcore is more complete than in many other drillcores from the East Baltic region.

Stable carbon-isotope trends versus sequence stratigraphy

In order to test whether the stable carbon-isotope curve can be used as a proxy for relative sea-level, the relation between the two is discussed below using the correlation between δ¹³C trends as proposed by Föllmi *et al.* (1994) and Vahrenkamp (1996). These authors suggested that distinct δ¹³C trends can be translated to corresponding sea-level trends and stacking patterns in the following way: (i) a positive δ¹³C trend correlates with

rising sea-level (TST with backstepping and condensed sections downdip); (ii) a constant $\delta^{13}C$ trend correlates with slack sea-level (HST with high carbonate production and aggradation and progradation); and (iii) a negative $\delta^{13}C$ trend correlates with falling sea-level (forced regression or LST, may be absent updip due to erosion). Because the core #9103 (Fig. 5) does not cover the upper part of the study succession, only the cores #9800 (Fig. 4) and #8010 (Fig. 6) are used to test the relation between the isotope trends and systems tracts within the sequences.

Overall, the gross facies stacking patterns and carbon-isotope trends within the upper Red River Formation do not show a clear covariance suggestive of a relation between the $\delta^{13}C$ trends and the relative sea-level changes. The major differences include the following: (i) the onset of drowning correlates fairly well with the positive $\delta^{13}C$ excursion at the base of RR1 in well #8010, but predates it in well #9800; (ii) the negative $\delta^{13}C$ trend of the LST part of RR2 is marked by deposition of anhydrite and dololaminite (well #8010) but, in well #9800, the negative trend continues through the subtidal TST of sequence RR2; (iii) the subsequent positive $\delta^{13}C$ trend ($\delta^{13}C$-derived TST) is not recorded at the same intervals in the two studied wells; (iv) the late TST and entire HST of the sequence RR2 in core #8010 are represented by an overall constant $\delta^{13}C$ value, while in core #9800, the HST contains a major positive followed by a negative excursion; and (v) the $\delta^{13}C$ trends from both cores differ in the sequence SM1, which prevents a breakdown of the SM1 on $\delta^{13}C$-derived systems tracts.

It should be noted that, when viewed in a global perspective, the relations between changes in sea-level and $\delta^{13}C$ trends (e.g. Föllmi *et al.*, 1994; Jenkyns, 1996; Vahrenkamp, 1996; Colombié *et al.*, 2011) are more complex than may appear locally. As shown by several authors (e.g. Bergström *et al.*, 2010c), the prominent Guttenberg excursion occurs in some areas (for example, Kentucky, Oklahoma) in highstand deposits, whereas in other regions (for example, south-eastern Norway and Estonia), it is present in lowstand units. The even more conspicuous Hirnantian isotope excursion, the largest positive excursion in the entire Ordovician, occurs within a well-known eustatic lowstand, which is recognized globally and interpreted to be caused by major glaciations in Gondwana. In the Cincinnati region, the top portion of the Elkhorn Formation with the beginning of the Elkhorn excursion clearly represents a regressive event that is followed by a very long

period of non-marine conditions. In the same region, as well as in Illinois, the Whitewater excursion is associated with a regressive event (cf. Goldman & Bergström, 1997). Hence, as shown by these and other examples, a clear relation between sea-level highstands and positive $\delta^{13}C$ excursions is not clear, and other factors, including regional environmental effects, coupled with diagenesis, are likely to be more important than vertical changes of the surface of the sea.

CONCLUSIONS

The upper Katian Red River Formation is an overall shallowing (and 'brining') upward supersequence reaching a thickness of more than 210 m in the epicratonic Williston Basin depocentre in North Dakota. The supersequence is composed of at least three long-term (third-order) depositional sequences that formed east of the very broad and shallow, tropical, arid carbonate shelf that developed east of the western passive margin of North America. The *ca* 87 m thick investigated interval in the upper part of the Red River Formation in North Dakota provides one of the most complete upper Katian (post-Waynesville excursion and pre-Hirnatian excursion) $\delta^{13}C$ records available in North America. The results of the present study may be summarized as follows:

1 $\delta^{13}C$ values of shallow-marine Red River carbonates vary from $-3‰$ to $+1.7‰$ in limestone and from $-0.7‰$ to $+2‰$ in dolomite; such similar values suggest that carbon was rock buffered and could be representing the original marine $\delta^{13}C$ record.

2 Fine crystal size, lack of zoning and non-obliterated porosity in the dolomites sampled for stable isotopes, coupled with their intimate association with the overlying evaporites, suggest a hypersaline-brine, early replacive origin for the bulk of the dolomite. Dark orange to red luminescence of both laminated and burrowed dolomites suggests their similar dolomitization history and diagenetic stabilization under reducing conditions.

3 The $\delta^{13}C$ trend of the study interval from the upper Red River Formation to the lowermost part of the Stony Mountain Formation can be subdivided into eight stages, with the Red River Formation being characterized by three major excursions to positive $\delta^{13}C$ values that can be correlated across the Williston Basin. The first excursion (stage II) with an amplitude of up to $+2‰$

occurs in the C laminated member. The second excursion (stage IV) reaches an amplitude of +2‰ within the B burrowed member. Both excursions occur within the upper Katian *Aphelognathus divergens* Conodont Zone. The third excursion (stage VI) with an amplitude of +2‰ to +4‰ occurs in the middle part of the A interval, above the A anhydrite or A laminite member.

4 With the help of conodont biostratigraphy, the Williston Basin δ^{13}C profiles can be correlated with the δ^{13}C profile reported from the Cincinnati region (Midcontinent, USA), coeval intervals in the Vauréal Formation on Anticosti Island (Québec) and in the Pirgu Stage of the East Baltic region. The chemostratigraphic correlation suggests that the upper Red River Formation is biostratigraphically above the upper part of *Amplexograptus manitolinensis* Graptolite Zone (lower part of *Amorphognathus ordovicicus* Conodont Zone); i.e. it is Late Katian in age. This is consistent with biostratigraphic evidence from shelly fossils and conodonts.

5 The different overall trend and absolute δ^{13}C values between the Williston Basin and the Cincinnati Region suggest a lack of exchange between waters of the Williston Basin and the Midcontinent and, consequently, the influence of different regional environmental processes characteristic of a large, periodically isolated Williston Basin, coupled with different diagenetic histories.

6 No clear relation can be established between the carbon-isotope trends and the relative sea-level changes based on gross facies stacking patterns, which suggests that the magnitude of δ^{13}C values was mainly controlled by factors other than water depth.

ACKNOWLEDGEMENTS

REFERENCES

Achab, A. (1977) Les chitinozoires de la zone à *Climacograptus prominens elongatus* de la Formation de Vauréal (Ordovicien supérieur), Ile d'Anticosti, Québec. *Can. J. Earth Sci.*, **14**, 2193–2212.

Achab, A., **Asselin, E.**, **Desrochers, A.**, **Riva, J.** and **Farley, C.** (2011) Chitinozoan biostratigraphy of a new Upper Ordovician stratigraphic framework for Anticosti Island, Canada. *Geol. Soc. Am. Bull.*, **123**, 186–205.

Ainsaar, T., **Meidla, T.** and **Martma, T.** (2004) The middle Caradoc facies and faunal turnover in the Late Ordovician Baltoscandian palaeobasin. *Palaeogeogr. Palaeoclimatol. Palaeoecol.*, **210**, 119–133.

Ainsaar, L., **Kaljo, D.**, **Martma, T.**, **Meidla, T.**, **Männik, T.**, **Nõlvak, J.** and **Tinn, O.** (2010) Middle and Upper Ordovician carbon isotope chronostratigraphy in Baltoscandia: a correlation standard and clues to environmental history. *Palaeogeogr. Palaeoclimatol. Palaeoecol.*, **294**, 189–201.

Allan, J.R. and **Matthews, R.K.** (1977) Carbon and oxygen isotopes as diagenetic and stratigraphic tools: surface and subsurface data, Barbados, West Indies. *Geology*, **5**, 16–20.

Allan, J.R. and **Matthews, R.K.** (1982) Isotope signatures associated with early meteoric diagenesis. *Sedimentology*, **29**, 797–817.

Alroy, J., **Aberhan Bottjer, M.D.J.**, **Foote, M.**, **Fursich, F. T.**, **Harries, P. J.**, **Hendy, A. J. W.**, **Holland, S. M.**, **Ivany, L. C.**, **Kiessling, W.**, **Kosnik, M.A.**, **Marshall, C.R.**, **McGowan, A.J.**, **Miller, A.I.**, **Olszewski, T.D.**, **Patzkowsky, M.E.**, **Peters, S.E.**, **Villier, L.**, **Wagner, P.J.**, **Bonuso, N.**, **Borkow, P.S.**, **Brenneis, B.**, **Clapham, M.E**, **Fall, L.M.**, **Ferguson, C.A.**, **Hanson, V.L.**, **Krug, A.Z.**, **Layou, K.M.**, **Leckey, E.H.**, **Nürnberg, S.**, **Powers, C.M.**, **Sessa, J.A.**, **Simpson, C.**, **Tomasovych, A.** and **Visaggi, C.C.** (2008) Phanerozoic trends in the global diversity of marine invertebrates. *Science*, **321**, 97–100.

Alsharhan, A.S. and **Sadd, J.L.** (2000) Stylolites in Lower Cretaceous carbonate reservoirs, U.A.E. In: *Middle East Models of Jurassic/Cretaceous Carbonate Systems* (Eds A.S. Alsharhan and R.W. Scott), *SEPM Spec. Publ.*, **69**, 185–207.

Anderson, T.F. and **Arthur, M.A.** (1983) Stable isotopes of oxygen and carbon and their application to sedimentologic and environmental problems. In: *Stable Isotopes in Sedimentary Geology* (Eds M.A. Arthur, T.F. Anderson, I.R. Kaplan, J. Veizer and L.S. Land). *SEPM Short Course Notes*, **10**, 1–151.

Ballard, F.V. (1963) Structural and stratigraphic relationships in the Paleozoic rocks of eastern North Dakota. *North Dakota Geol. Surv. Bull.*, **20**, 42.

Banner, J.L., **Hanson, G.N.** and **Meyers, W.J.** (1988) Water-rock interaction history of regionally extensive dolomites of the Burlington-Keokuk Formation (Mississippian): isotopic evidence. In: *Sedimentology and Geochemistry of Dolostones* (Eds V. Shukla and P.A. Baker), *SEPM Spec. Publ.*, **43**, 97–114.

Bergström, S.M., Young, S., Schmitz, B. and Saltzman, M.R. (2007) Upper Ordovician (Katian) $\delta^{13}C$ chemostratigraphy: a trans-Atlantic comparison. *Acta Palaeontol. Sinica*, **46** (Suppl.), 37–39.

Bergström, S.M., Chen, X., Guttiérrez-Marco, J.C. and Dronov, A. (2009) The new chronostratigraphic classification of the Ordovician system and its relations to major regional series and stages and $\delta^{13}C$ chemostratigraphy. *Lethaia*, **42**, 97–107.

Bergström, S.M., Calner, M., Lehnert, O. and Noor, A. (2010a) A new upper Middle Ordovician-Lower Silurian drillcore standard succession from Borenshult in Östergötland, southern Sweden. 1. Stratigraphical review with regional comparisons. *GFF*, **133**, 149–171.

Bergström, S.M., Lehnert, O., Calner, M. and Joachimski, M.M. (2010b) A new upper Middle Ordovician-Lower Silurian drillcore standard succession from Borenshult in Östergötland, southern Sweden: 2. Significance of $\delta^{13}C$ chemostratigraphy. *GFF*, **134**, 39–63.

Bergström, S.M., Schmitz, B., Saltzman, M.R. and Huff, W.D. (2010c) The Upper Ordovician Guttenberg $\delta^{13}C$ excursion (GICE) in North America and Baltoscandia: occurrence, chronostratigraphic significance, and paleoenvironmental relationships. In: *The Ordovician Earth System* (Eds S.C. Finney and W.B.N. Berry), *GSA Spec. Pap.*, **466**, 37–67.

Bergström, S.M., Young, S. and Schmitz, B. (2010d) Katian (Upper Ordovician) $\delta^{13}C$ chemostratigraphy and sequence stratigraphy in the United States and Baltoscandia: a regional comparison. *Palaeogeogr. Palaeoclimatol. Palaeoecol.*, **296**, 217–234.

Bergström, S.M., Eriksson, M.E., Young, S.A., Ahlberg, P. and Schmitz, B. (2014) Hirnantian (latest Ordovician) $\delta^{13}C$ chemostratigraphy in southern Sweden and globally: a refined integration with the graptolite and conodont zone successions. *GFF*, **136**, 355–386.

Berner, R.A. (1994) GEOCARB II: a revised model of atmospheric CO_2 over Phanerozoic time. *Am. J. Sci.*, **294**, 56–91.

Berner, R.A. and Kothavala, Z. (2001) GEOCARB III: a revised model of atmospheric CO_2 over Phanerozoic time. *Am. J. Sci.*, **301**, 182–204.

Bluemle, J.P., Anderson, S.B. and Carlson, C.G. (1981) Williston Basin stratigraphic nomenclature chart. *North Dakota Geol. Surv. Misc. Ser.*, **61**, 1 pl.

Boyd, D.W. (2007) Morphology and diagenesis of *Dimorphosiphon talbotorium* n. sp., an Ordovician skeleton-building alga (Chlorophyta: Dimorphosiphonaceae). *J. Paleontol.*, **81**, 1–8.

Brasier, M.D., Corfield, R.M., Derry, L.A., Rozanov, A.Yu. and Zhuravlev, A.Yu. (1994) Multiple $\delta^{13}C$ excursions spanning the Cambrian explosion to the Botomian crisis in Siberia. *Geology*, **22**, 455–458.

Brenchley, P.J., Marshall, J.D., Carden, G.A.F., Robertson, D.B.R., Long, D.G.F., Meidla, T., Hints, L. and Anderson, T.F. (1994) Bathymetric and isotopic evidence for a short-lived Late Ordovician glaciation in a greenhouse period. *Geology*, **22**, 295–298.

Brenchley, P.J., Carden, G.A., Hints, L., Kaljo, D., Marshall, J.D., Martma, T., Meidla, T. and Nõlvak, J. (2003) High-resolution stable isotope stratigraphy of Upper Ordovician sequences: constraints on the timing of bioevents and environmental changes associated with mass extinction and glaciation. *Geol. Soc. Am. Bull.*, **115**, 89–104.

Calvert, S.E., Bustin, R.P. and Ingall, E.D. (1996) Influence of water column anoxia and sediment supply on the burial and preservation of organic carbon in marine shales. *Geochim. Cosmochim. Acta*, **60**, 1577–1593.

Canter, K.L. (1998) Facies, cyclostratigraphic and secondary diagenetic controls on reservoir distribution, Ordovician Red River Formation, Midale Field, southern Saskatchewan. In: *Eighth International Williston Basin Symposium, Core Workshop* (Ed. L.K. Kreis), pp. 41–65. Saskatchewan, North Dakota & Montana Geological Societies, Regina.

Carlson, C.G. and Anderson, S.B. (1965) Sedimentary and tectonic history of North Dakota part of Williston Basin. *AAPG Bull.*, **49**, 1833–1846.

Carroll, W.K. (1979) Depositional environments and paragenetic porosity controls, upper Red River Formation, North Dakota. *North Dakota Geol. Surv. Rep. Inv.*, **66**, 51.

Chafetz, H.S., Imerito-Tetzlaff, A.A. and Zhang, J. (1999) Stable-isotope and elemental trends in Pleistocene sabkha dolomites: descending meteoric waters vs. sulfate reduction. *J. Sed. Res.*, **69**, 268–278.

Christ, N., Immenhauser, A., Amour, F., Mutti, M., Preston, R., Whitacker, F.F., Peterhänsel, A., Egenhoff, S.O., Dunn, P.A. and Agar, S.M. (2012) Triassic Latemar cycle tops – subaerial exposure of platform carbonates under tropical arid climate. *Sed. Geol.*, **265–266**, 1–29.

Clement, J.H. (1987) Cedar Creek: a significant paleotectonic feature of the Williston Basin. In: *Williston Basin: Anatomy of a Cratonic Oil Province* (Ed. M.W. Longman), pp. 323–336. Rocky Mountain Association of Geologists, Denver.

Colombié, C., Lécuyer, C. and Strasser, A. (2011) Carbon- and oxygen-isotope records of palaeoenvironmental and carbonate production changes in shallow-marine carbonates (Kimmeridgian, Swiss Jura). *Geol. Mag.*, **148**, 133–153.

Copper, P. (2001) Reefs during multiple crises toward the Ordovician-Silurian boundary, Anticosti Island, eastern Canada, and world-wide. *Can. J. Earth Sci.*, **38**, 153–171.

Cummings, C.E. and McCarthy, H.B. (1982) Stable carbon isotope ratios in *Astrangea danae:* evidence for algal modification of varbon pools used in calcification. *Geochim. Cosmochim. Acta*, **46**, 1125–1129.

Curtis, C.D., Petrowski, C. and Oertel, G. (1972) Stable carbon isotope ratios within carbonate concretions: a clue to place and time of formation. *Nature*, **235**, 98–100.

Demski, M.W., Wheadon, B.J., Stewart, L.A., Elias, R.J., Young, G.A., Nowlan, G.S. and Dobrzanskyt, E.P. (2011) Ordovician-Silurian boundary interval in the Williston and Hudson Bay basins, Manitoba: isotopic carbon excursion and conodont turnover. Geol. Assoc. Can. Annu. Meet., Abstracts. Ottawa, Canada, pp. 50–51.

Derby, J.R. and Kilpatrick, J.T. (1985) Ordovician Red River dolomite reservoirs, Killdeer Field, North Dakota. In: *Carbonate Petroleum Reservoirs* (Eds P.O. Roehl and P.W. Choquette), pp. 61–69. Springer-Verlag, New York.

Derry, L.A., Kaufman, A.J. and Jacobsen, S.B. (1992) Sedimentary cycling and environmental change in the Late Proterozoic: evidence from stable and radiogenic isotopes. *Geochim. Cosmochim. Acta*, **56**, 1317–1329.

Dickson, J.A.D., Wood, R.A., Al Rougha, H.B. and Shebl, H. (2008) Sulphate reduction associated with hardgrounds: lithification afterburn! *Sed. Geol.*, **205**, 34–39.

Elias, R.J., Nowlan, G.S. and Bolton, T.E. (1988) Paleontology of the type section, Fort Garry Member, Red River Formation (Upper Ordovician), southern Manitoba. In: *Contributions to Paleozoic Paleontology in Honor of*

Rousseau H. Flower (Ed. D.L. Wohlberg), *Bull. New Mex. Bur. Min. Mineral Resour.*, **44**, 341–359.

Finnegan, S., Bergmann, K., Eiler, J.M., Jones, D.S., Fike, D.A., Eisenman, I., Hughes, N.C., Tripati, A.K. and Fischer, W.W. (2011) The magnitude and duration of Late Ordovician-Early Silurian glaciation. *Science*, **331**, 903–906.

Fischer, A.G. (1982) Long term climate oscillations recorded in stratigraphy. In: *Climate in Earth History* (Eds W.H. Berger and J.C. Crowell), pp. 97–104. National Academic Press, Washington DC.

Föllmi, K.B., Weissert, H., Bisping, M. and Funk, H. (1994) Phosphogenesis, carbon-isotope stratigraphy, and carbonate-platform evolution along the Lower Cretaceous northern Tethyan margin. *Geol. Soc. Am. Bull.*, **106**, 729–746.

Frakes, L.A. (1979) *Climates Throughout Geologic Time.* Elsevier, Amsterdam, 310 pp.

Frakes, L.A., Francis, J.E. and Syktus, J.I. (1992) *Climate Modes of the Phanerozoic: The History of the Earth's Climate Over the Past 600 Million Years.* Cambridge University Press, Cambridge, 274 pp.

Fuller, J.G.C.M. (1961) Ordovician and continuous formations in North Dakota. *AAPG Bull.*, **45**, 1334–1363.

Garrels, R.M. and Christ, C.L. (1965) *Solutions, Minerals and Equilibria.* Freeman, San Francisco, 450 pp.

Gerhard, L.C., Anderson, S.B., LeFever, J.A. and Carlson, C.G. (1982) Geological development, origin, and energy mineral resources of Williston basin, North Dakota. *AAPG Bull.*, **66**, 989–1020.

Gerhard, L.C., Anderson, S.B. and LeFever, J.A. (1987) Structural history of the Nesson anticline. In: *Williston Basin: Anatomy of a Cratonic Oil Province* (Ed. M.W. Longman), pp. 337–353. Rocky Mountain Association of Geologists, Denver.

Gingras, M.K., Pemberton, S.G., Muelenbachs, K. and Machel, H. (2004) Conceptual models for burrow-related, selective dolomitization with textural and isotopic evidence from the Tyndall Stone, Canada. *Geobiology*, **2**, 21–30.

Gischler, E., Swart, P.K. and Lomando, A.J. (2009) Stable isotopes of carbon and oxygen in modern sediments of carbonate platforms, Barrier Reefs, Atolls and Ramps: patterns and implications. In: *Perspectives in Carbonate Geology: A Tribute to the Career of Robert Nathan Ginsburg* (Eds P.K. Swart, G.P. Eberli and J.A. McKenzie), *Int. Assoc. Sedimentol. Spec. Publ.*, **41**, 61–74.

Glumac, B. and Walker, K.R. (1998) A Late Cambrian positive carbon-isotope excursion in the Southern Appalachians: relation to biostratigraphy, sequence stratigraphy, environments of deposition, and diagenesis. *J. Sed. Res.*, **68**, 1212–1222.

Goldman, D. and Bergström, S.M. (1997) Late Ordovician graptolites from the North American Midcontinent. *Palaeontology*, **40**, 965–1010.

Herrmann, A.D., Haupt, B.J., Patzkowsky, M.E., Seidov, D. and Slingerland, R.L. (2004) Response of Late Ordovician paleoceanography to changes in sea level, continental drift, and atmospheric pCO$_2$: potential causes for long-term cooling and glaciation. *Palaeogeogr. Palaeoclimatol. Palaeoecol.*, **210**, 385–401.

Hite, R.J. and Buckner, D.H. (1981) Stratigraphic correlations, facies concepts, and cyclicity in Pennsylvanian rocks of the Paradox Basin. In: *Geology of the Paradox Basin, 1981 Field Conference* (Ed. D.L. Weigand), pp. 147–159. Rocky Mountain Association of Geologists, Denver.

Holland, S.M. and Patzkowsky, M.E. (2009) Stratigraphic architecture of a tropical carbonate platform and its effect on the distribution of fossils: Ordovician Bighorn Dolomite, Wyoming, USA. *Palaios*, **24**, 303–317.

Holmden, C. (2009) Ca isotope study of Ordovician dolomite, limestone, and anhydrite in the Williston Basin: implications for subsurface dolomitization and local Ca cycling. *Chem. Geol.*, **268**, 180–188.

Husinec, A. (2013) Sedimentary evolution of Williston Basin at the onset of Hirnantian glaciation. Geol. Soc. Am. Annu. Conven., Abstracts with Program. Denver, CO, USA, 243 pp.

Husinec, A. and Read, J.F. (2011) Microbial laminite versus rooted and burrowed caps on peritidal cycles: salinity control on parasequence development, Early Cretaceous isolated carbonate platform, Croatia. *Geol. Soc. Am. Bull.*, **123**, 1896–1907.

Immenhauser, A., Della Porta, G., Kenter, J.A.M. and Bahamonde, J.E. (2003) An alternative model for positive shifts in shallow-marine carbonate δ^{13}C and δ^{18}O. *Sedimentology*, **50**, 953–959.

Immenhauser, A., Holmden, C. and Patterson, W.P. (2008) Interpreting the carbon-isotope record of shallow epeiric seas: lessons from the recent. In: *Dynamics of Epeiric Seas* (Eds B.R. Pratt and C. Holmden), *Geol. Assoc. Can. Spec. Publ.*, **48**, 135–174.

Jenkyns, H.C. (1996) Relative sea-level change and carbon isotopes: data from the Upper Jurassic (Oxfordian) of central and Southern Europe. *Terra Nova*, **8**, 75–85.

Jenkyns, H.C., Jones, C.E., Gröcke, D.R., Hesselbo, S.P. and Parkinson, D.N. (2002) Chemostratigraphy of the Jurassic System: applications, limitations and implications for palaeoceanography. *J. Geol. Soc. London*, **159**, 351–378.

Jin, J. (2000) Evolution and extinction of the North American *Hiscobeccus* brachiopod Fauna during the Late Ordovician. *Can. J. Earth Sci.*, **38**, 143–151.

Jin, J. and Zhan, R.-B. (2001) *Late Ordovician Articulate Brachiopods from the Red River and Stony Mountain Formations.* National Research Council of Canada Research Press, Ottawa, Southern Manitoba, 117 pp.

Jin, J., Harper, D.A.T., Cocks, L.R.M., McCausland, P.J.A., Rasmussen, C.M.Ø. and Sheehan, P. (2013) Precisely locating the Ordovician equator in Laurentia. *Geology*, **41**, 107–110.

Jones, D.S., Fike, D.A., Finnegan, S., Fisher, W.W., Schrag, D.P. and McCay, D. (2011) Terminal Ordovician carbon isotope stratigraphy and glacioeustatic sea-level change across Anticosti Island (Québec, Canada). *Geol. Soc. Am. Bull.*, **123**, 1645–1664.

Kaljo, D., Hints, L., Martma, T., Nõlvak, J. and Oraspõld, A. (2004) Late Ordovician carbon isotope trend in Estonia, its significance in stratigraphy and environmental analysis. *Palaeogeogr. Palaeoclimatol. Palaeoecol.*, **210**, 165–185.

Kaljo, D., Hints, L., Männik, P. and Nõlvak, J. (2008) The succession of Hirnantian events based on data from Baltica: brachiopods, chitinozoans, conodonts, and carbon isotopes. *Est. J. Earth Sci.*, **57**, 197–218.

Kaufman, A.J., Jacobsen, S.B. and Knoll, A.H. (1993) The Vendian record of Sr and C isotopic variations in seawater: implications for tectonics and paleoclimate. *Earth Planet. Sci. Lett.*, **120**, 409–430.

Kendall, A.C. (1976) *The Ordovician Carbonate Succession (Bighorn Group) of Southeastern Saskatchewan.* Saskatchewan Geological Survey, Department of Mineral Resources, Report, 190, 185 pp.

Kohm, J.A. and Louden, R.O. (1978) Ordovician Red River of Eastern Montana-western North Dakota: relationships

between lithofacies and production. Montana Geological Society 24th Annual Field Conference Guidebook, pp. 99–117.

Kump, L.R., Arthur, M.A., Patzkowsky, M.E., Gibbs, M.T., Pinkus, D.S. and Sheehan, P.M. (1999) A weathering hypothesis for glaciation at high atmospheric pCO_2 during the Late Ordovician. *Palaeogeogr. Palaeoclimatol. Palaeoecol.*, **152**, 173–187.

Lashkov, E.M. and Paškevičius, J. (1989) The stratigraphic gaps and sedimentation breaks of the Ordovician section in the western borderland of the East European platform. In: *Nauchnye Trudy Vyshikh uchebnykh zavedeniy Litovskoi SSR, Geologija*, **10**, 12–37 (In Russian).

Lee, D. and Carpenter, S.J. (2001) Isotopic disequilibrium in marine calcareous algae. *Chem. Geol.*, **172**, 307–329.

LeFever, R.D., Thompson, S.C. and Anderson, D.B. (1987) Earliest Paleozoic history of the Williston Basin in North Dakota. In: *Fifth International Williston Basin Symposium* (Eds C.G. Carlson and J.E. Christopher), *Sask. Geol. Soc. Spec. Publ.*, **9**, 22–37.

Lespérance, P.J. (1982) Field Meeting Anticosti-Gaspé, Québec, 1981, vol. II, Stratigraphy and Paleontology, IUGS Subcommission on Silurian Stratigraphy and Ordovician-Silurian Boundary Working Group. Département de Géologie, Université de Montréal, 321 pp.

Lohmann, K.C. (1988) Geochemical pattern of meteoric diagenetic systems and their application to the study of paleokarst. In: *Paleokarst* (Eds N.P. James and P.W. Choquette), pp. 58–80. Springer-Verlag, New York.

Longman, M.W., Fertal, T.G. and Glennie, J.S. (1983) Origin and geometry of Red River dolomite reservoirs, western Williston Basin. *AAPG Bull.*, **67**, 744–771.

Loyd, M.R. (1964) Variations in the oxygen and carbon isotope ratios of Florida Bay mollusks and their environmental significance. *J. Geol.*, **72**, 84–111.

Lucia, F.J. and Major, R.P. (1994) Porosity evolution through hypersaline reflux dolomitization. In: *Dolomites, a Volume in Honour of Dolomieu* (Eds B.H. Purser, M.E. Tucker and D.H. Zenger), *Int. Assoc. Sedimentol. Spec. Publ.*, **21**, 325–341.

Ludvigson, G.A., Jacobson, S.R., Witzke, B.J. and Gonzalez, L.A. (1996) Carbonate component chemostratigraphy and depositional history of the Ordovician Decorah Formation, Upper Mississippi Valley. In: *Paleozoic Sequence Stratigraphy: Views From the North American Craton* (Eds B.J. Witzke, G.A. Ludvigson and J. Day), *Geol. Soc. Am. Spec. Pap.*, **306**, 67–86.

Ludvigson, G.A., Witzke, B.J., González, L.A., Carpenter, S.J., Schneider, C.L. and Hasiuk, F. (2004) Late Ordovician (Turinian–Chatfieldian) carbon isotope excursions and their stratigraphic and paleoceanographic significance. *Palaeogeogr. Palaeoclimatol. Palaeoecol.*, **210**, 187–214.

Machel, H.G. (1999) Effects of groundwater flow on mineral diagenesis, with emphasis on carbonate aquifers. *Hydrogeol. J.*, **7**, 94–107.

Machel, H.G. and Burton, E.A. (1991) Factors governing cathodoluminescence in calcite and dolomite and their implications for studies of carbonate diagenesis. In: *Luminescence Microscopy: Qualitative and Quantitative Applications* (Eds C.E. Barker and O.C. Kopp), *SEPM Short Course Notes*, **25**, 37–57.

Marshall, J.D., Brenchley, P.J., Mason, P., Wolff, G.A., Astini, R.A., Hints, L. and Meidla, T. (1997) Global carbon isotopic events associated with mass extinction and glaciation in the late Ordovician. *Palaeogeogr. Palaeoclimatol. Palaeoecol.*, **132**, 195–210.

McConnaughey, T. (1989) ^{13}C and [18]O isotopic disequilibrium in biological carbonates: I. Patterns. *Geochim. Cosmochim. Acta*, **53**, 151–162.

McCracken, A.D. and Barnes, C.R. (1981) Conodont biostratigraphy and palaeoecology of the Ellis Bay Formation, Anticosti Island, Quebec, with special reference to late Ordovician-early Silurian chronostratigraphy and the systemic boundary. *Bull. Geol. Surv. Can.*, **329**, 51–134.

McKenzie, J.A. (1981) Holocene dolomitization of calcium carbonate sediments from the coastal sabkas of Abu Dhabi, U.A.E. *J. Geol.*, **89**, 185–198.

McLaughlin, P.I., Emerson, N., Witzke, B., Sell, B. and Emsbo, P. (2011) Distal signatures of Late Ordovician oceanic anoxia – new data from a classic epeiric ramp transect. In: *Archean to Anthropocene: Field Guides to the Geology of Mid-Continent North America* (Eds J.D. Miller, G.J. Hudak, C. Wittkop and P.I. McLaughlin), *Geol. Soc. Am. Field Guide*, **24**, 259–284.

Melim, L.A. and Scholle, P.A. (2002) Dolomitization of the Capitan Formation forereef facies (Permian, west Texas and New Mexico): seepage reflux revisited. *Sedimentology*, **49**, 1207–1227.

Montanez, I.P. (1997) Secondary porosity and late diagenetic cements of the Upper Knox Group, central Tennessee region: a temporal and spatial history of fluid flow conduit development within the Knox regional aquifer. In: *Basin-Wide Diagenetic Patterns: Integrated Petrologic, Geochemical, and Hydologic Considerations* (Eds I.P. Montanez, J.M. Gregg and K.L. Shelton), *SEPM Spec. Publ.*, **57**, 101–117.

Montanez, I.P. and Read, J.F. (1992) Fluid-rock interaction history during stabilization of early dolomites, Upper Knox Group (Lower Ordovician), U.S. Appalachians. *J. Sed. Petrol.*, **62**, 753–778.

Moore, C.H., Chowdhury, A. and Chan, L. (1988) Upper Jurassic Smackover platform dolomitization, northwestern Gulf of Mexico: a tale of two waters. In: *Sedimentology and Geochemistry of Dolostones* (Eds V. Shukla and P.A. Baker), *SEPM Spec. Publ.*, **43**, 175–189.

Morrow, D.W. (1982) Diagenesis 1. Dolomite – part 1: the geochemistry of dolomitization and dolomite precipitation. *Geosci. Can.*, **9**, 5–13.

Mountjoy, E.W., Machel, H.G., Green, D., Duggan, J. and Williams-Jones, A.E. (1999) Devonian matrix dolomites and deep burial carbonate cements: a comparison between the Rimbey-Meadowbrook reef trend and the deep basin of west-central Alberta. *Bull. Can. Petrol. Geol.*, **47**, 487–509.

Murphy, E.C., Nordeng, S.H., Juenker, B.J. and Hoganson, J.W. (2009) Stratigraphic column of North Dakota. *North Dakota Geol. Surv. Misc. Ser.*, **91**, 1 pl.

Neese, D.E. (1985) Depositional environment and diagenesis of the Red River Formation, "C" Interval, Divide County, North Dakota and Sheridan County, Montana. In: *Rocky Mountain Carbonate Reservoirs* (Eds M.W. Longman, K.W. Shanley, R.F. Lindsay and D.E. Eby), *SEPM Core Workshop*, **7**, 95–124.

Nowlan, G.S. and Barnes, C.R. (1981) Late Ordovician conodonts from the Vauréal Formation, Anticosti Island, Québec. *Bull. Geol. Surv. Can.*, **329**, 1–49.

Oberg, R. (1966) Winnipeg conodonts from Manitoba. *J. Paleontol.*, **40**, 130–147.

Oehlert, A.M., Lamb-Wozniak, K.A., Devlin, Q.B., MacKenzie, G.J., Reijmer, J.J. and Swart, P.K. (2012) The stable carbon isotopic composition of organic material in

platform derived sediments: implications for reconstructing the global carbon cycle. *Sedimentology*, **59**, 319–335.

Panchuk, K., **Holmden, C.E.** and **Kump, L.R.** (2005) Sensitivity of the epeiric sea carbon isotope record to local-scale carbon cycle processes: tales from the Mohawkian Sea. *Palaeogeogr. Palaeoclimatol. Palaeoecol.*, **228**, 320–337.

Panchuk, K., **Holmden, C.E.** and **Leslie, S.A.** (2006) Local controls on carbon cycling in the Ordovician Midcontinent region of North America with implications for carbon isotope secular curves. *J. Sed. Res.*, **76**, 200–211.

Paris, F., **Elaouad-Debbaj, Z.**, **Jaglin, J.C.**, **Massa, D.** and **Oulebsir, L.** (1995) Chitinozoans and Late Ordovician glacial events on Gondwana. In: *Ordovician Odyssey: Short Papers for the Seventh International Symposium on the Ordovician System* (Eds D. Cooper, M.L. Droser and S.L. Finney), pp. 171–176. Pacific Section SEPM, Fullerton, California.

Patterson, W.P. and **Walter, L.M.** (1994) Depletion of ^{13}C in seawater ΣCO_2 on modern carbonate platforms: significance for the carbon isotopic record of carbonates. *Geology*, **22**, 885–888.

Patzkowsky, M.E., **Slupik, L.M.**, **Arthur, M.A.**, **Pancost, R.D.** and **Freeman, K.H.** (1997) Late Middle Ordovician environmental change and extinction: harbinger of the Late Ordovician or continuation of Cambrian patterns? *Geology*, **25**, 911–914.

Pope, M.C. and **Read, J.F.** (1998) Ordovician meter-scale cycles: implications for climate and eustatic fluctuations in the central Appalachians during a global greenhouse, non-glacial to glacial transition. *Palaeogeogr. Palaeoclimatol. Palaeoecol.*, **138**, 27–42.

Porter, J.W. and **Fuller, J.G.C.M.** (1959) Lower Paleozoic rocks of northern Williston basin and adjacent areas. *AAPG Bull.*, **43**, 124–189.

Qing, H. and **Veizer, J.** (1994) Oxygen carbon isotopic composition of Ordovician brachiopods; implications for coeval seawater. *Geochim. Cosmochim. Acta*, **58**, 4429–4442.

Qing, H., **Kent, D.** and **Bend, S.** (2001) Preliminary results of isotopic geochemistry of Ordovician Red River carbonates, subsurface of southeastern Saskatchewan: implication for process of dolomitization and diagenetic modification of dolomites. Summary of Investigations 2001. Saskatchewan Geological Survey; Saskatchewan Energy and Mines, Miscellaneous Report 2001-4-1,1, 3–9.

Railsback, L.B., **Holland, S.M.**, **Hunter, D.E.**, **Michael, E.J.**, **Diaz, J.R.** and **Crowe, D.E.** (2003) Controls on geochemical expression of subaerial exposure in Ordovician limestones from the Nashville Dome, Tennessee, U.S.A. *J. Sed. Res.*, **73**, 790–805.

Rendall, B.E. and **Husinec, A.** (2012) Importance of *Dimorphosiphon* (Chlorophyta, Bryopsidales) for facies and biostratigraphic studies of the Upper Ordovician Richmondian Red River Formation, Williston Basin. *Palaios*, **27**, 713–725.

Riva, J. (1969) Middle and Upper Ordovician graptolite faunas of Saint Lawrence Lowlands of Quebec and Anticosti Island. In: *North Atlantic-Geology and Continental Drift: A Symposium* (Ed. M. Kay), *AAPG. Mem.*, **12**, 513–556.

Saltzman, M.R. and **Young, S.A.** (2005) Long-lived glaciation in the Late Ordovician? Isotopic and sequence-stratigraphic evidence from western Laurentia. *Geology*, **33**, 109–112.

Sandberg, C.A. (1964) Precambrian to Mississippian paleotectonics of the southern Williston basin. 3rd International Williston Basin Symposium, Proceedings, pp. 37–38.

Sarg, J.F. (1988) Carbonate sequence stratigraphy. In: *Sea-Level Changes: An Integrated Approach* (Eds C.K. Wilgus, B.S. Hastings, C.G.St.C. Kendall, H.W. Posamentier, C.A. Ross and J.C. Van Wagoner), *SEPM Spec. Publ.*, **42**, 155–181.

Sarg, J.F. (2001) The sequence stratigraphy, sedimentology, and economic importance of evaporite-carbonate transitions: a review. *Sed. Geol.*, **140**, 9–42.

Sarg, J.F., **Suriamin, K.T.M.** and **Humphrey, J.D.** (2013) Lithofacies, stable isotopic composition, and stratigraphic evolution of microbial and associated carbonates, Green River Formation (Eocene), Piceance Basin, Colorado. *AAPG Bull.*, **97**, 1937–1966.

Sass, E., **Bein, A.** and **Almogi-Labin, A.** (1991) Oxygen-isotope composition of diagenetic calcite in organic-rich rocks: evidence for ^{18}O depletion in marine anaerobic pore water. *Geology*, **19**, 839–842.

Schidlowski, M. (1979) Carbon isotope geochemistry of the 3.7×10^9 yr-old Isua sediments, West Greenland: implications for the Archean carbon and oxygen cycles. *Geochim. Cosmochim. Acta*, **43**, 189–199.

Sepkoski, J.J. (1995) The Ordovician radiations: diversification and extinction shown by global genus-level taxonomic data. In: *Ordovician Odyssey: Short Papers for the Seventh International Symposium on the Ordovician System* (Eds D. Cooper, M.L. Droser and S.L. Finney), pp. 393–396. Pacific Section SEPM, Fullerton, California.

Shackleton, N.J. and **Pisias, N.G.** (1985) Atmospheric carbon dioxide, orbital forcing, and climate. In: *The Carbon Cycle and atmospheric CO2: Natural Variations Archaen to Present: Geophysical Monograph* (Eds E.T. Sundquist and W.S. Broecker), pp. 412–417. AGU, Washington D.C.

Sheehan, P.M. (2001) The Late Ordovician mass extinction. *Annu. Rev. Earth Planet. Sci.*, **29**, 331–364.

Sinclair, G.W. (1959) Succession of Ordovician rocks in southern Manitoba. *Geol. Surv. Can. Pap.*, **59–5**, 5.

Skoglund, R. (1963) Uppermost Viruan and Lower Harjuan (Ordovician) stratigraphy of Västergötland and Lower Harjuan graptolite faunas of central Sweden. *Bull. Geol. Inst. Univ. Uppsala*, **42**, 1–55.

Sloss, L.L. (1963) Sequences in the cratonic interior of North America. *Geol. Soc. Am. Bull.*, **74**, 93–114.

Swart, P.K. (1983) Carbon and oxygen isotope fractionation in Scleractinian corals: a review. *Earth Sci. Rev.*, **19**, 51–80.

Swart, P.K. and **Eberli, G.P.** (2005) The nature of the δ^{13}C of periplatform sediments: implications for stratigraphy and the global carbon cycle. *Sed. Geol.*, **175**, 115–129.

Swart, P.K. and **Kennedy, M.J.** (2012) Does the global stratigraphic reproducibility of δ^{13}C in Neoproterozoic carbonates require a marine origin? A Pliocene-Pleistocene comparison. *Geology*, **40**, 87–90.

Swart, P.K. and **Melim, L.A.** (2000) The origin of dolomites in Tertiary sediments from the margin of Great Bahama Bank. *J. Sed. Res.*, **70**, 738–748.

Swart, P.K., **Reijmer, J.G.** and **Otto, R.** (2009) A re-evaluation of facies on Great Bahama Bank II: variations in the d13C, d18O and mineralogy of surface sediments. In: *Perspectives in Carbonate Geology: A Tribute to the Career of Robert Nathan Ginsburg* (Eds P.K. Swart, G.P. Eberlie and J.A. McKenzie), *Int. Assoc. Sedimentol. Spec. Publ.*, **41**, 47–59.

Sweet, W.C. (1982) Conodonts from the Winnipeg Formation (Middle Ordovician) of the northern Black Hills, South Dakota. *J. Paleontol.*, **56**, 1029–1059.

Tobin, K.J. and **Walker, K.R.** (1997) Ordovician oxygen isotopes and paleotemperatures. *Palaeogeogr. Palaeoclimatol. Palaeoecol.*, **129**, 269–290.

Trotter, J.A., **Williams, I.S.**, **Barnes, C.R.**, **Lécuyer, C.** and **Nicoll, R.S.** (2008) Did cooling oceans trigger Ordovician biodiversification? Evidence from conodont thermometry. *Science*, **321**, 550–554.

Tucker, M.E. (1991) Sequence stratigraphy of carbonate-evaporite basins: models and application to the Upper Permian (Zechstein) of Northeast England and adjoining North Sea. *J. Geol. Soc. London*, **148**, 1019–1036.

Twenhofel, W.H. (1929) Geology of Anticosti Island. *Can. Geol. Surv. Mem.*, **154**, 1–481.

Underwood, C.J., **Crowley, S.**, **Marshall, J.D.** and **Brenchley, P.J.** (1997) High-resolution carbon isotope stratigraphy of the basal Silurian stratotype (Dob's Linn, Scotland) and its global correlation. *J. Geol. Soc. London*, **154**, 709–718.

Vahrenkamp, V.C. (1996) Carbon isotope stratigraphy of the Upper Kharaib and Shuaiba formations: implications for the Early Cretaceous evolution of the Arabian Gulf Region. *AAPG Bull.*, **80**, 647–662.

Vahrenkamp, V.C. and **Swart, P.K.** (1994) Late Cenozoic dolomites of the Bahamas: metastable analogues for the genesis of ancient platform dolomites. In: *Dolomites, a Volume in Honor of Dolomieu* (Eds B. Purser, M. Tucker and D. Zenger), *Int. Assoc. Sedimentol. Spec. Publ.*, **21**, 133–153.

Van Wagoner, J.C., **Posamentier, H.W.**, **Mitchum, R.M. Jr**, **Vail, P.R.**, **Sarg, J.F.**, **Loutit, T.S.** and **Hardenbol, J.** (1988) An overview of the fundamentals of sequence stratigraphy and key definitions. In: *Sea-Level Changes: An Integrated Approach* (Eds C.K. Wilgus, B.S. Hastings, C.G.St.C. Kendall, H.W. Posamentier, C.A. Ross and J.C. Van Wagoner), *SEPM Spec. Publ.*, **42**, 39–47.

Vandenbroucke, T.R.A., **Armstrong, H.A.**, **Williams, M.**, **Paris, F.**, **Zalasiewicz, J.A.**, **Sabbe, K.**, **Nõlvak, J.**, **Challands, T.J.**, **Verniers, J.** and **Servais, T.** (2010) Polar front shift and atmospheric CO2 during the glacial maximum of the Early Paleozoic Icehouse. *Proc. Natl Acad. Sci. USA*, **107**, 14983–14986.

Vasconcelos, C., **McKenzie, J.A.**, **Warthmann, R.** and **Bernasconi, S.M.** (2005) Calibribration of the $\delta^{18}O$ paleothermometer for dolomite precipitated in microbial cultures and natural environments. *Geology*, **33**, 317–320.

Veizer, J. and **Hoefs, J.** (1976) The nature of $^{18}O/^{16}O$ and $^{13}C/^{12}C$ secular trends in sedimentary carbonate rocks. *Geochim. Cosmochim. Acta*, **40**, 1387–1395.

Weber, L.J., **Sarg, J.F.** and **Wright, F.M.** (1995) Sequence stratigraphy and reservoir delineation of the Middle Pennsylvanian (Desmoinesian) Paradox basin and Aneth Field, southwestern USA. In: *Milankovitch Sea-Level Changes, Cycles, and Reservoirs on Carbonate Platforms in Greenhouse and Ice-House Worlds* (Eds J.F. Read, C. Kerans, L.J. Weber, J.F. Sarg and F.M. Wright), *SEPM Short Course Notes*, **35**, 1–81.

Weissert, H. (1989) C-isotope stratigraphy, a monitor of paleoenvironmental change: a case study from the early Cretaceous. *Surv. Geophys.*, **10**, 1–61.

Yapp, C.J. and **Poths, H.** (1992) Ancient atmospheric CO_2 pressures inferred from natural goethites. *Nature*, **355**, 342–344.

Young, S.A., **Saltzman, M.R.**, **Ausich, W.I.**, **Desrochers, A.** and **Kaljo, D.** (2010) Did changes in atmospheric CO_2 coincide with latest Ordovician glacial–interglacial cycles? *Palaeogeogr. Palaeoclimatol. Palaeoecol.*, **296**, 376–388.

Zenger, D.H. (1996) Dolomitization of the "C" zone, Red River Formation (Upper Ordovician) in a deep core, Williston basin, Richland County, eastern Montana. *Contrib. Geol.*, **31**, 57–75.

APPENDIX

Table A1. Borehole data for logged intervals and bulk matrix samples.

Well name	NDIC[a] No.	County	Latitude	Longitude	Elevation[b] in metres (feet)	Red River top[§]	Logged interval top[c]	Logged interval bottom[§]	Logged interval thickness	Samples
Urlacher State Unit #1	8010	Hettinger	46°18′25.47″N	102°48′23.19″W	816.3 (2678)	3070.9 (10075)	3069.9 (10072)	3156.5 (10356)	86.6 (284)	101
Federal #10-1	9103	Dunn	47°33′46.57″N	102°53′28.07″W	668.4 (2193)	4170.9 (13684)	4192.8 (13756)	4267.8 (14002)	75 (246)	69
Simpson #1	9800	Williams	48°28′46.10″N	103°11′51.60″W	694 (2277)	4045.9 (13274)	4041.6 (13260)	4113.9 (13497)	72.2 (237)	65

Cores are stored at the North Dakota Geological Survey's Wilson M. Laird Core and Sample Library, Grand Forks, North Dakota. [a] North Dakota Industrial Commission, Oil and Gas Division. [b] Referenced to the kelly bushing (KB), an adapter that serves to connect the rotary table to the kelly. [c] Depth below the KB in metres (feet).

Table A2. Stable-isotope data for bulk carbonate matrix samples.

Depth (m)	Depth (feet)	δ^{13}C [‰ VPDB]	δ^{18}O [‰ VPDB]	Bulk Lithology	Interval/Member	Formation
NDGS #8010[a]						
3070.6	10074	0.75	−6.77	Limestone		Stony Mountain
3071.5	10077	0.08	−7.40	Limestone		Stony Mountain
3072.4	10080	−0.33	−7.35	Limestone		Stony Mountain
3073.3	10083	−0.63	−7.00	Limestone	A interval	Red River
3073.9	10085	−1.05	−5.81	Limestone	A interval	Red River
3074.5	10087	−1.12	−6.11	Limestone	A interval	Red River
3075.4	10090	−1.87	−5.93	Limestone	A interval	Red River
3076.3	10093	−0.30	−5.55	Limestone	A interval	Red River
3077.0	10095	−0.59	−4.17	Dolomite	A interval	Red River
3077.6	10097	−0.09	−4.24	Dolomite	A interval	Red River
3077.9	10098	−0.95	−5.61	Limestone	A interval	Red River
3078.8	10101	−0.24	−4.75	Limestone	A interval	Red River
3079.7	10104	−0.30	−5.09	Limestone	A interval	Red River
3080.6	10107	−0.34	−5.49	Limestone	A interval	Red River
3081.5	10110	−0.20	−4.70	Limestone	A interval	Red River
3082.4	10113	−1.39	−4.83	Limestone	A interval	Red River
3083.1	10115	−2.08	−4.59	Limestone	A interval	Red River
3084.0	10118	−2.00	−4.49	Limestone	A interval	Red River

Table A2. (continued)

Depth (m)	Depth (feet)	δ¹³C [‰ VPDB]	δ¹⁸O [‰ VPDB]	Bulk Lithology	Interval/Member	Formation
3084.9	10121	−0.92	−4.95	Limestone	A interval	Red River
3087.3	10129	1.27	−4.91	Dolomite	B laminated mbr.	Red River
3087.9	10131	1.33	−5.13	Dolomite	B laminated mbr.	Red River
3088.2	10132	1.43	−5.14	Dolomite	B laminated mbr.	Red River
3088.5	10133	1.07	−4.94	Dolomite	B laminated mbr.	Red River
3089.8	10137	0.96	−3.89	Dolomite	B laminated mbr.	Red River
3090.7	10140	0.73	−6.03	Limestone	B burrowed mbr.	Red River
3091.3	10142	0.71	−5.33	Limestone	B burrowed mbr.	Red River
3092.2	10145	1.13	−5.44	Limestone	B burrowed mbr.	Red River
3093.1	10148	0.79	−6.77	Limestone	B burrowed mbr.	Red River
3094.0	10151	0.90	−5.64	Limestone	B burrowed mbr.	Red River
3095.2	10155	0.93	−5.31	Limestone	B burrowed mbr.	Red River
3096.2	10158	0.72	−4.11	Limestone	B burrowed mbr.	Red River
3097.1	10161	1.14	−5.09	Limestone	B burrowed mbr.	Red River
3098.0	10164	0.78	−5.30	Limestone	B burrowed mbr.	Red River
3098.9	10167	0.78	−5.05	Limestone	B burrowed mbr.	Red River
3099.8	10170	1.36	−5.17	Limestone	B burrowed mbr.	Red River
3100.7	10173	0.99	−5.07	Limestone	B burrowed mbr.	Red River
3101.6	10176	−0.74	−4.33	Limestone	B burrowed mbr.	Red River
3105.3	10188	0.34	−4.79	Dolomite	C anhydrite mbr.	Red River
3106.2	10191	0.32	−4.58	Dolomite	C anhydrite mbr.	Red River
3107.1	10194	−0.03	−4.56	Dolomite	C anhydrite mbr.	Red River
3108.0	10197	−0.69	−4.18	Dolomite	C anhydrite mbr.	Red River
3109.3	10201	0.53	−4.46	Dolomite	C anhydrite mbr.	Red River
3109.9	10203	1.08	−4.02	Dolomite	C anhydrite mbr.	Red River
3110.2	10204	0.46	−4.43	Dolomite	C anhydrite mbr.	Red River
3111.1	10207	0.28	−4.37	Dolomite	C anhydrite mbr.	Red River
3111.4	10208	−0.04	−4.41	Dolomite	C anhydrite mbr.	Red River
3112.0	10210	0.68	−4.60	Dolomite	C laminated mbr.	Red River
3112.9	10213	0.89	−4.72	Dolomite	C laminated mbr.	Red River
3113.5	10215	1.52	−4.70	Dolomite	C laminated mbr.	Red River
3113.8	10216	0.87	−4.70	Dolomite	C laminated mbr.	Red River
3114.4	10218	0.70	−4.63	Dolomite	C laminated mbr.	Red River
3115.1	10220	1.18	−5.06	Dolomite	C laminated mbr.	Red River
3115.4	10221	0.78	−4.86	Dolomite	C laminated mbr.	Red River
3116.3	10224	0.65	−5.53	Dolomite	C laminated mbr.	Red River
3117.5	10228	0.21	−6.33	Limestone	C laminated mbr.	Red River
3118.4	10231	1.03	−4.11	Dolomite	C laminated mbr.	Red River
3119.3	10234	1.12	−4.57	Dolomite	C laminated mbr.	Red River
3120.2	10237	0.92	−6.11	Limestone	C laminated mbr.	Red River

Table A2. (continued)

Depth (m)	Depth (feet)	δ¹³C [‰ VPDB]	δ¹⁸O [‰ VPDB]	Bulk Lithology	Interval/Member	Formation
3120.5	10238	0.48	−6.40	Limestone	C laminated mbr.	Red River
3121.5	10241	0.63	−6.43	Limestone	C laminated mbr.	Red River
3122.4	10244	0.71	−6.38	Limestone	C laminated mbr.	Red River
3123.3	10247	1.50	−5.18	Dolomite	C laminated mbr.	Red River
3124.5	10251	1.25	−4.93	Dolomite	C laminated mbr.	Red River
3125.1	10253	1.04	−4.57	Dolomite	C laminated mbr.	Red River
3125.7	10255	1.04	−4.23	Dolomite	C laminated mbr.	Red River
3126.6	10258	0.54	−5.70	Limestone	C burrowed mbr.	Red River
3127.6	10261	0.30	−6.36	Limestone	C burrowed mbr.	Red River
3128.5	10264	0.13	−6.01	Limestone	C burrowed mbr.	Red River
3129.4	10267	0.10	−6.59	Limestone	C burrowed mbr.	Red River
3130.3	10270	0.60	−6.25	Limestone	C burrowed mbr.	Red River
3131.2	10273	−0.01	−6.71	Limestone	C burrowed mbr.	Red River
3132.1	10276	0.22	−6.57	Limestone	C burrowed mbr.	Red River
3133.0	10279	0.35	−6.30	Limestone	C burrowed mbr.	Red River
3134.0	10282	0.25	−5.94	Limestone	C burrowed mbr.	Red River
3134.9	10285	0.14	−6.32	Limestone	C burrowed mbr.	Red River
3135.8	10288	0.37	−6.68	Limestone	C burrowed mbr.	Red River
3136.7	10291	0.42	−6.37	Limestone	C burrowed mbr.	Red River
3137.6	10294	0.20	−5.93	Limestone	C burrowed mbr.	Red River
3138.2	10296	1.05	−3.78	Dolomite	C burrowed mbr.	Red River
3138.5	10297	0.43	−5.71	Dol. limestone	C burrowed mbr.	Red River
3139.1	10299	0.66	−5.30	Dolomite	C burrowed mbr.	Red River
3140.0	10302	0.60	−5.49	Limestone	C burrowed mbr.	Red River
3141.0	10305	0.09	−6.47	Limestone	C burrowed mbr.	Red River
3141.9	10308	0.27	−6.31	Limestone	C burrowed mbr.	Red River
3143.7	10314	0.28	−7.21	Limestone	C burrowed mbr.	Red River
3144.3	10316	1.08	−4.58	Dolomite	C burrowed mbr.	Red River
3145.5	10320	0.47	−6.63	Limestone	C burrowed mbr.	Red River
3147.1	10325	0.21	−7.14	Limestone	C burrowed mbr.	Red River
3152.9	10344	0.53	−5.78	Limestone	C burrowed mbr.	Red River
3153.8	10347	0.11	−6.28	Limestone	C burrowed mbr.	Red River
3154.7	10350	0.74	−5.18	Limestone	C burrowed mbr.	Red River
3155.6	10353	0.36	−5.68	Limestone	C burrowed mbr.	Red River
3156.5	10356	0.39	−6.07	Limestone	C burrowed mbr.	Red River

Table A2. (continued)

Depth (m)	Depth (feet)	$\delta^{13}C$ [‰ VPDB]	$\delta^{18}O$ [‰ VPDB]	Bulk Lithology	Interval/Member	Formation
NDGS #9103						
4194.7	13762	1.71	−6.72	Limestone	B anhydrite mbr.	Red River
4195.6	13765	1.29	−6.96	Limestone	B laminite mbr.	Red River
4196.5	13768	1.15	−4.94	Dolomite	B laminite mbr.	Red River
4197.4	13771	0.26	−5.65	Dolomite	B laminite mbr.	Red River
4198.0	13773	0.59	−5.31	Dolomite	B laminite mbr.	Red River
4198.6	13775	0.30	−4.91	Limestone	B laminite mbr.	Red River
4215.1	13829	1.22	−4.72	Dolomite	C anhydrite mbr.	Red River
4216.0	13832	−0.20	−5.28	Dolomite	C anhydrite mbr.	Red River
4217.2	13836	1.11	−5.51	Dolomite	C laminated mbr.	Red River
4217.5	13837	1.32	−4.66	Dolomite	C laminated mbr.	Red River
4217.8	13838	0.88	−4.91	Dolomite	C laminated mbr.	Red River
4218.7	13841	0.79	−5.06	Dolomite	C laminated mbr.	Red River
4219.3	13843	0.45	−4.72	Dolomite	C laminated mbr.	Red River
4219.7	13844	0.10	−5.27	Dolomite	C laminated mbr.	Red River
4223.9	13858	−0.23	−6.45	Limestone	C laminated mbr.	Red River
4224.8	13861	0.19	−6.16	Limestone	C laminated mbr.	Red River
4225.7	13864	−0.11	−6.70	Limestone	C laminated mbr.	Red River
4226.7	13867	−0.02	−6.80	Limestone	C burrowed mbr.	Red River
4227.6	13870	0.10	−6.79	Limestone	C burrowed mbr.	Red River
4228.5	13873	−0.09	−6.83	Limestone	C burrowed mbr.	Red River
4229.1	13875	0.49	−6.14	Limestone	C burrowed mbr.	Red River
4230.3	13879	−0.10	−6.29	Limestone	C burrowed mbr.	Red River
4230.9	13881	0.21	−6.26	Limestone	C burrowed mbr.	Red River
4231.8	13884	0.45	−5.35	Dolomite	C burrowed mbr.	Red River
4232.8	13887	0.25	−6.84	Dolomite	C burrowed mbr.	Red River
4233.7	13890	0.44	−5.36	Limestone	C burrowed mbr.	Red River
4234.0	13891	0.32	−4.88	Dolomite	C burrowed mbr.	Red River
4234.6	13893	0.00	−6.15	Limestone	C burrowed mbr.	Red River
4235.5	13896	0.11	−6.56	Limestone	C burrowed mbr.	Red River
4236.4	13899	0.65	−5.24	Limestone	C burrowed mbr.	Red River
4236.7	13900	0.75	−5.38	Dolomite	C burrowed mbr.	Red River
4237.3	13902	0.20	−6.57	Dolomite	C burrowed mbr.	Red River
4238.2	13905	0.00	−6.65	Limestone	C burrowed mbr.	Red River
4239.2	13908	0.07	−6.59	Limestone	C burrowed mbr.	Red River
4240.1	13911	0.34	−6.07	Limestone	C burrowed mbr.	Red River
4241.0	13914	0.42	−5.74	Limestone	C burrowed mbr.	Red River
4242.2	13918	0.54	−6.00	Limestone	C burrowed mbr.	Red River
4243.1	13921	−0.36	−6.78	Limestone	C burrowed mbr.	Red River
4244.0	13924	0.56	−5.79	Limestone	C burrowed mbr.	Red River

Table A2. (continued)

Depth (m)	Depth (feet)	δ¹³C [‰ VPDB]	δ¹⁸O [‰ VPDB]	Bulk Lithology	Interval/Member	Formation
4244.6	13926	0.93	−5.42	Dolomite	C burrowed mbr.	Red River
4244.9	13927	0.18	−6.15	Limestone	C burrowed mbr.	Red River
4245.9	13930	−0.02	−6.30	Limestone	C burrowed mbr.	Red River
4246.8	13933	−0.09	−6.29	Limestone	C burrowed mbr.	Red River
4247.7	13936	0.03	−5.81	Limestone	C burrowed mbr.	Red River
4248.9	13940	0.23	−6.06	Limestone	C burrowed mbr.	Red River
4249.5	13942	0.88	−4.96	Dolomite	C burrowed mbr.	Red River
4249.8	13943	0.21	−5.81	Limestone	C burrowed mbr.	Red River
4250.7	13946	0.10	−5.85	Limestone	C burrowed mbr.	Red River
4252.0	13950	0.11	−5.96	Limestone	C burrowed mbr.	Red River
4252.9	13953	0.15	−5.82	Limestone	C burrowed mbr.	Red River
4253.8	13956	0.37	−5.63	Limestone	C burrowed mbr.	Red River
4254.7	13959	−0.10	−5.93	Limestone	C burrowed mbr.	Red River
4255.6	13962	0.58	−5.69	Limestone	C burrowed mbr.	Red River
4256.5	13965	−0.06	−5.40	Limestone	C burrowed mbr.	Red River
4257.4	13968	0.29	−5.44	Limestone	C burrowed mbr.	Red River
4258.4	13971	−0.15	−6.16	Limestone	C burrowed mbr.	Red River
4259.3	13974	0.48	−6.16	Limestone	C burrowed mbr.	Red River
4259.9	13976	0.46	−6.71	Limestone	C burrowed mbr.	Red River
4260.8	13979	0.35	−6.06	Limestone	C burrowed mbr.	Red River
4261.7	13982	0.78	−5.69	Limestone	C burrowed mbr.	Red River
4262.6	13985	0.38	−6.25	Limestone	C burrowed mbr.	Red River
4263.5	13988	0.50	−5.61	Limestone	C burrowed mbr.	Red River
4264.2	13990	0.93	−5.76	Limestone	C burrowed mbr.	Red River
4265.1	13993	1.09	−5.97	Limestone	C burrowed mbr.	Red River
4266.0	13996	0.83	−6.15	Limestone	C burrowed mbr.	Red River
4266.6	13998	0.97	−6.07	Limestone	C burrowed mbr.	Red River
4267.5	14001	0.77	−6.17	Limestone	C burrowed mbr.	Red River
NDGS #9800						
4042.6	13263	−0.90	−6.83	Limestone		Stony Mountain
4043.5	13266	−0.87	−6.47	Limestone		Stony Mountain
4044.4	13269	−2.79	−7.43	Limestone		Stony Mountain
4045.6	13273	−0.67	−6.26	Limestone	A interval	Red River
4046.2	13275	−0.23	−5.73	Limestone	A interval	Red River
4047.1	13278	−2.03	−5.99	Limestone	A interval	Red River
4048.0	13281	0.04	−6.17	Limestone	A interval	Red River
4049.0	13284	−0.13	−6.51	Limestone	A interval	Red River
4049.9	13287	0.31	−6.54	Limestone	A interval	Red River
4051.1	13291	−0.32	−6.62	Limestone	A interval	Red River
4052.0	13294	−0.83	−5.67	Limestone	A interval	Red River

Table A2. (continued)

Depth (m)	Depth (feet)	δ13C [‰ VPDB]	δ18O [‰ VPDB]	Bulk Lithology	Interval/Member	Formation
4052.6	13296	1.05	−3.78	Limestone	A interval	Red River
4052.9	13297	−3.07	−5.85	Limestone	A interval	Red River
4053.8	13300	−1.31	−6.02	Limestone	A interval	Red River
4056.9	13310	−0.71	−6.27	Limestone	A interval	Red River
4057.8	13313	−1.78	−4.84	Limestone	A interval	Red River
4059.6	13319	−1.33	−5.35	Limestone	A interval	Red River
4060.5	13322	−2.50	−6.22	Limestone	A interval	Red River
4060.9	13323	−1.80	−6.42	Limestone	A interval	Red River
4061.5	13325	−2.67	−6.70	Limestone	A interval	Red River
4062.4	13328	−2.09	−6.24	Limestone	A interval	Red River
4063.3	13331	−2.41	−5.77	Limestone	A interval	Red River
4064.2	13334	−2.45	−5.11	Limestone	A interval	Red River
4066.0	13340	−0.44	−7.51	Dolomite	B anhydrite mbr.	Red River
4069.7	13352	0.99	−4.35	Dolomite	B laminated mbr.	Red River
4070.6	13355	1.77	−5.32	Dolomite	B laminated mbr.	Red River
4071.2	13357	2.06	−4.59	Dolomite	B laminated mbr.	Red River
4071.5	13358	1.64	−4.89	Dolomite	B laminated mbr.	Red River
4071.8	13359	0.43	−5.08	Dolomite	B laminated mbr.	Red River
4072.4	13361	0.54	−5.60	Dolomite	B laminated mbr.	Red River
4074.3	13367	0.37	−6.51	Limestone	B burrowed mbr.	Red River
4075.2	13370	−0.99	−5.43	Limestone	B burrowed mbr.	Red River
4076.1	13373	−0.14	−5.41	Limestone	B burrowed mbr.	Red River
4077.0	13376	0.46	−5.66	Limestone	B burrowed mbr.	Red River
4077.3	13377	0.59	−6.11	Limestone	B burrowed mbr.	Red River
4077.9	13379	0.04	−6.90	Limestone	B burrowed mbr.	Red River
4078.8	13382	0.65	−6.45	Limestone	B burrowed mbr.	Red River
4080.7	13388	0.47	−4.98	Limestone	B burrowed mbr.	Red River
4084.9	13402	−0.03	−6.64	Dolomite	C anhydrite mbr.	Red River
4085.8	13405	1.20	−4.56	Dolomite	C anhydrite mbr.	Red River
4087.1	13409	0.97	−7.75	Dolomite	C anhydrite mbr.	Red River
4089.8	13418	0.75	−8.04	Limestone	C laminated mbr.	Red River
4090.7	13421	0.51	−6.17	Limestone	C laminated mbr.	Red River
4091.6	13424	−0.03	−7.41	Limestone	C laminated mbr.	Red River
4092.2	13426	−1.01	−7.89	Limestone	C laminated mbr.	Red River
4093.5	13430	0.01	−6.46	Limestone	C laminated mbr.	Red River
4094.1	13432	−0.12	−7.17	Limestone	C laminated mbr.	Red River
4095.0	13435	−0.15	−6.79	Limestone	C laminated mbr.	Red River
4095.9	13438	−0.69	−7.59	Limestone	C laminated mbr.	Red River
4096.8	13441	0.40	−5.10	Limestone	C laminated mbr.	Red River
4097.4	13443	−0.98	−7.75	Limestone	C laminated mbr.	Red River

Table A2. (continued)

Depth (m)	Depth (feet)	δ¹³C [‰ VPDB]	δ¹⁸O [‰ VPDB]	Bulk Lithology	Interval/Member	Formation
4098.3	13446	−0.38	−7.02	Limestone	C laminated mbr.	Red River
4099.3	13449	−0.47	−7.89	Limestone	C laminated mbr.	Red River
4099.9	13451	0.00	−6.95	Limestone	C laminated mbr.	Red River
4100.8	13454	0.30	−7.22	Limestone	C laminated mbr.	Red River
4102.6	13460	−0.45	−7.82	Limestone	C laminated mbr.	Red River
4103.5	13463	0.32	−5.90	Limestone	C laminated mbr.	Red River
4105.4	13469	−0.04	−6.07	Limestone	C laminated mbr.	Red River
4106.0	13471	−0.27	−6.72	Limestone	C laminated mbr.	Red River
4108.4	13479	−0.21	−6.11	Limestone	C laminated mbr.	Red River
4109.3	13482	−0.17	−7.41	Limestone	C laminated mbr.	Red River
4110.2	13485	−0.27	−6.30	Limestone	C laminated mbr.	Red River
4111.8	13490	0.97	−4.50	Limestone	C laminated mbr.	Red River

ᵃNorth Dakota Industrial Commission, Oil and Gas Division; well no.